ELSEVIER

Contents lists available at ScienceDirect

Acta Astronautica

journal homepage: www.elsevier.com/locate/actaastro



Research paper

Towards robotic on-orbit assembly of large space telescopes: Mission architectures, concepts, and analyses

Angadh Nanjangud ^{a,b,*}, Craig Underwood ^c, Chakravarthini M. Rai ^d, Steve Eckersley ^e, Martin Sweeting ^{c,e}, Paolo Bianco ^f

- a Queen Mary University of London, London, E1 4NS, United Kingdom
- b Space HQ Ltd, London, EC1V 8DN, United Kingdom
- ^c Surrey Space Centre, University of Surrey, Guildford, GU2 7XH, United Kingdom
- ^d University of Lincoln, Lincolnshire, LN6 7TS, United Kingdom
- ^e Surrey Satellite Technology Limited, Guildford, GU2 7YE, United Kingdom
- f Airbus, Anchorage Road, Portsmouth, PO3 5PU, United Kingdom

ARTICLE INFO

Keywords: On-orbit assembly Space mission architecture Large space telescopes Space robotics

ABSTRACT

Imaging systems larger than the James Webb Space Telescope will enable unprecedented astronomy in the future. Larger aperture space-based imagers will also support next-generation Earth Observation missions for national security and disaster monitoring. However, launching and operating such large telescopes in the poses several practical challenges. A key challenge is that mirrors with apertures larger than 3 m cannot be monolithically manufactured so a segmented design is utilized to achieve primary mirror apertures. Even if larger mirrors could be made, it would be impossible to stow them in fairings of most existing and future launch vehicles. Folded-wing designs to deploy segmented primary mirrors, as done with the James Webb Space Telescope, are one approach to overcoming this volumetric challenge but inappropriate for 25 m apertures considered in this study. This paper presents the concept of operations and mission architectures/analysis for on-orbit assembly of a 25 m aperture telescope operating in the visible waveband of the electromagnetic spectrum capable of 1 m spatial resolution from geostationary orbit. Further, a technology demonstration roadmap towards maturing the robotic assembly technology stack is then presented as precursors to the 25 m imaging system.

1. Introduction

The Hubble Space Telescope (HST) and James Webb Space Telescope (JWST) are two prominent modern-day space telescopes; the latter is one of the first to employ a segmented mirror design for space astronomy to overcome the challenges of stowing in a launch vehicle. Larger aperture space telescopes than JWST will require multiple launches and autonomous on-orbit assembly technologies [1] to assemble them so as to enable next generation space astronomy [2] and persistent Earth Observation [3]. While Lee et al. [2] considered the use of robots assembling a telescope at the Sun-Earth Lagrange Point 2 (SEL2), Saunders [3] proposed the use of free-flyer satellites to realize large Earth observation (EO) imagers.

The years following these studies has seen an uptick in interest to assemble astronomical space telescopes at SEL2. In mid-2018, NASA's Science Mission Directorate initiated the year-long in-Space Assembled Telescope (iSAT) study [4] to learn when in- space assembly of observatories offers better value than launching monolithic telescopes

in a single launch vehicle. Contributions from a substantial team of 70 subject experts from various NASA centres, academia, government laboratories/agencies, and industry determined that observatories with aperture diameters larger than 15 m could only be achieved using in-space assembly. A corresponding whitepaper was submitted to the National Academies' Astro2020 Decadal Survey [5].

Robotically assembling SEL2 telescopes also emerged in Europe with the European Space Agency (ESA) MIRROR project [6]; their approach was to build on the developments from a number of earlier European projects:

- H2020 Space Robotics projects such as MOSAR [7], SIROM [8], PULSAR [9,10] and HOTDOCK [11],
- ESA ISS EUROBOT project [12], and
- ESA TRP Dexterous Robot Arm (DEXARM) [13].

https://doi.org/10.1016/j.actaastro.2024.08.022

Received 8 March 2024; Received in revised form 13 July 2024; Accepted 14 August 2024 Available online 23 August 2024

^{*} Corresponding author at: Queen Mary University of London, London, E1 4NS, United Kingdom. E-mail address: a.nanjangud@qmul.ac.uk (A. Nanjangud).

The focus on the European side has primarily been on developing common building block technologies that can be used in various mission scenarios relevant to In-space Servicing, Assembly and Manufacturing (ISAM) where space telescope assembly is one use-case.

A large space observatory assembled on-orbit by a robot principally comprises four fundamental systems:

- 1. Optical Telescope Assembly (OTA) system,
- 2. Robotic Agent for Space Telescope Assembly (RASTA) system,
- 3. Base spacecraft (SC) system, and
- 4. Sunshield.

The focus of this paper is on item 1, the OTA system, which is shown in Fig. 3. Our justification for this focus is that the initial design drivers for EO telescope systems are subtly different from those of astronomy telescopes. The starting point for studies on astronomical telescopes is aperture size for the PM e.g., NASA studies into assembling 100 m [2] and smaller telescopes [14] and recent work in Europe on assembling telescopes [9,10,15]. On the other hand, EO telescope designs start with user requirements such as frequency of observation (in our case, the desire is 'persistent' observation of a location on Earth), the desired resolution, and the wavelength for observation must both meet the enduser's goals. As will be shown in Section 2, these become the inputs to determine the PM aperture size and operational orbit, which drive designs of robotics assemblers and spacecraft as well as selection of launch vehicles. The contrast in drivers makes sense for astronomy systems where bigger is generally better for science. Also, the choice of operational orbits can also be more flexible for astronomy as it is decoupled from resolution to some extent; a more important driver is the lighting conditions for imaging which becomes the reason for operating at the Sun-Earth Lagrange Point 2. Lastly, decisions made in achieving large astronomy telescopes developed by government space agencies appear less constrained by cost than EO systems developed by industry; for example, astronomy systems can be launched using the largest launch vehicles which may not necessarily be the most cost

Our paper is similar in terms of its focus to the works of Lee [2] and Saunders [3] in that we are exploring the architecture to realizing these systems via in-orbit assembly. Surrey Satellite Technology Limited (SSTL)'s interest in persistent high resolution EO from geostationary orbit underpins our work and differentiates it from Lee et al.'s focus on space astronomy. We also propose to use a lower cost philosophy for robotics and relying on designs with space heritage [16]. For example, their study considered using multi-limbed space robots for assembly requiring dual-arm manipulation and multi-legged locomotion [2] whereas we rely on single-arm manipulation systems based on the Space Station Remote Manipulator System (SSRMS) and other International Space Station (ISS) robotic systems. Single-arm manipulation was also assumed in the iSAT study [14]. Recent ground-based experiments by the PULSAR project [10] demonstrate sub-millimeter positioning accuracy when using standardized connectors such as the HOTDOCK [11]. This is not to imply that single-manipulator systems are superior in any way as there are many aspects to consider in evaluating the complex tradespace of choosing the appropriate robotic agent; this is out of the scope of this paper but the authors have attempted to evaluate various architectures [16] though more detailed analyses are needed. For example, examinations into the task-specific robot dynamics during truss assembly [17]. The broad area of ISAM is particularly pertinent to this research and one with a large number of players; a thorough piece on its current state of developments across world can be found in [18].

As mentioned above, our study more closely aligns with that of Saunders' for SSTL [3] with its focus on Earth imaging. However, our work is distinct from theirs in that we fully develop architectures using robotic in-space assembly of the EO system as opposed to free-flying satellite technology [19]. Further, we also dive deeper into the structural design aspects of the telescope from which we derive detailed

costs of subsystems that then feeds into the developing mission architectures and roadmapping several technology demonstration missions. Thus, we present a systems engineering perspective on enabling high resolution imaging of distant objects with large aperture telescopes via robotic assembly on-orbit. Within the scope of this study, the definition of "distant" refers to the altitude of an EO satellite located at GEO and the corresponding definition of "high resolution" is 1 m for such a telescope. The system will operate in the visible waveband of the electromagnetic spectrum ($\lambda=0.4$ –0.75 µm) and are thus also referred to as "optical" telescopes. This defines the "user requirement" for this study leading to the need for a 25 m aperture primary mirror. An artistic render of this study's 25 m aperture space telescope being assembled relevant is shown in Fig. 1.

The layout of our paper is as follows. We begin by translating the user requirements, defined above, into the requirements of the OTA; this is covered in Section 2. Requirements associated with the RASTA systems were presented in an earlier study evaluating various options for robotic assembly agents [16]. With a baseline telescope design and chosen robotic system, a mission architecture for assembling telescopes on-orbit is presented and analysed in Section 3. Then Section 4 proposes and analyses three demonstration mission concepts and Section 5 concludes this paper.

2. Space telescope design

Optical telescopes are typically classified under the following three categories-refracting, reflecting, and catadioptric telescopes. Refractor telescopes are uncommon in large telescopes as they suffer from chromatic aberrations at apertures over 1 m. As a result, reflecting systems are more common in space-based optical imaging, which can be further sub-classified based on the number of mirrors as single-mirror or multi-mirror telescopes. Introduction of corrector lenses into multi-mirror reflector designs leads to the aforementioned catadioptric design. This study limits consideration to reflecting telescopes given their more prominent use in contemporary space-based astronomy.

The next subsection presents a telescope design to meet user-defined requirements. We begin by translating high-level user requirements into appropriate optical parameters. Then, a discussion on the engineering trade-offs of various reflecting telescope designs leads us to an acceptable design for Earth Observation; the telescope's subsystems-level design is then further detailed.

2.1. From user requirements to optical system requirements

In the context of this study, aperture size and focal length of an imaging system are collectively referred to as the optical system requirements. They are calculated from the user requirements: 1 m spatial resolution from GEO (36,000 km is assumed to be suitable as an approximation of the defined GEO altitude of 35,876 km) in the visible wavelength of the electromagnetic spectrum.

Aperture size: The aperture size of a telescope system is dependent on two parameters: the wavelength at which observations are to be recorded and the desired angular resolution. First, the angular resolution (θ) is determined from the desired spatial resolution (r) and altitude of observation (h) as:

$$\theta = \frac{r}{h} = \frac{1 \text{ m}}{36,000 \text{ km}} = 2.78 \times 10^{-8} \text{ radians}$$
 (1)

Then, using the mid-band wavelength of the visible spectrum (λ = 0.55 μ m), the aperture size (D) is found to be 24.13 m using the Rayleigh criteria, as shown below:

$$D = 1.22 \frac{\lambda}{\theta} = 24.13 \text{ m}$$
 (2)

Choosing a 25 m aperture for the primary mirror (PM) gives a slightly larger light collecting area. Note that for diffraction-limited performance at the red-end of the visible spectrum ($\lambda=0.70~\mu m$), the

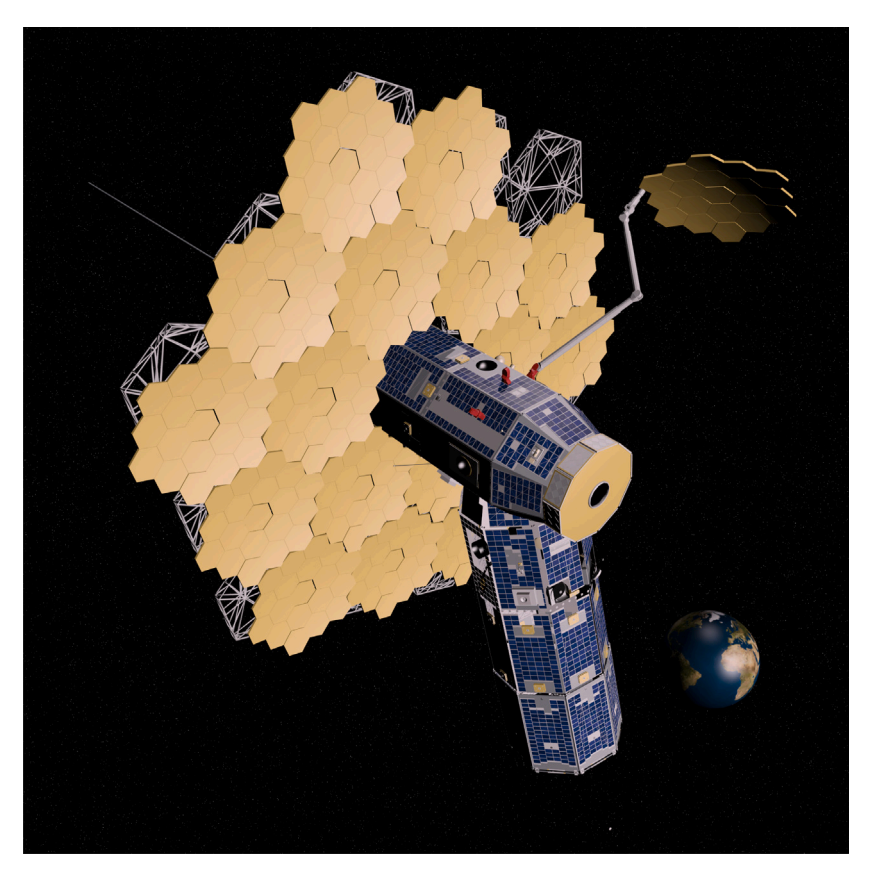


Fig. 1. Concept art depicting the assembly of a segmented PM of a 25 m space telescope by a robotic manipulator.

necessary aperture is ${\sim}30$ m; however, in keeping with user requirements as stated in [3], the telescope is assumed to be diffraction-limited at 0.55 μm .

Focal length: Determining focal length requires first selecting an appropriate detector to be located at the image plane. To this end, the Focal Plane Assembly (FPA) is assumed to consist of a grid of complementary metal–oxide–semiconductor (CMOS) detectors; the assumed CMOS sensor for the calculations presented here is based on the Teledyne-E2V Emerald 16M [20]. We assume each detector has 4096×4096 pixels, (i.e., 16 megapixels), where each pixel is a square of side 1.4 μ m. The effective focal length, f, to achieve the desired magnification (i.e., one pixel to be equivalent to 1 m on the ground) from GEO is given by:

$$\frac{f}{h} = \frac{x}{r}$$
 (3) where,

h, altitude of telescope = 36,000 km,

x, pixel cell size = $1.4 \mu m$, and

r, distance to be resolved = 1 m;

leading to $f=50.4~\rm m$. In other words, achieving a 1 m ground spatial resolution with a Newtonian focus (i.e., single-mirror assembly) requires a physical separation between the PM and the FPA of up to 50.4 m. A Newtonian focus is one where there are no secondary optics; the image is formed at the focal point of the PM. For space imaging, a single structure of this length would typically be a deployable that offers nanometre-level deployment precision. Upon deployment, the structure would further have to guarantee alignment errors between the FPA and PM to be within tens of nanometres [21]. Both challenges are yet to be overcome by current space technologies, which eliminates adopting single-mirror telescope designs for those that 'fold' the optics with multiple mirrors.

A Cassegrain focus is a common folded-optical design comprising two mirrors with the focus lying behind the PM. The classic Cassegrain configuration uses a parabolic primary reflector and a hyperbolic SM. Some of its other design variants are:

- 1. R-C telescope: In this design, both mirrors are hyperbolic to eliminate spherical aberrations and coma but off-axis astigmatism is an undersirable consequence. However, it is the most commonly used design in large professional-grade research telescopes and, notably, adopted by the HST.
- 2. **Schmidt-Cassegrain design**: This is a catadioptric version of Cassegrain; it uses a spherical PM and a Schmidt corrector plate (an aspheric lens) to correct for the spherical aberration. This design is preferred for its compactness and use of simple spherical optics. Most notably, this was used on the Kepler space telescope.
- 3. **Maksutov–Cassegrain design**: Also a catadioptric Cassegrain system with spherical mirrors; it is distinguishable by its full-aperture spherical meniscus corrector lens, more easily manufactured than a Schmidt plate. The lens helps eliminate coma and aberrations (spherical and chromatic).

Three-mirror anastigmat designs are another multi-mirror alternatative with three curved mirrors to minimize spherical aberration, coma, and astigmatism. They allow wider fields of view than telescopes with one or two mirrors. A variant of this design, called the Korsch telescope, is used in the JWST. A considerable disadvantage is that the increased mirrors count makes alignment far more complex than in two-mirror designs. This challenge is compounded when we account for the fact that the GEO imager requires on-orbit assembly (OOA) thus making it an undesirable choice.

As highlighted earlier, the ~ 50 m separation for single-mirror Newtonian designs is an unprecedented challenge for optical space telescopes. The Cassegrain system's folded optics allows uses a more compact geometric design without compromising the necessary overall (or

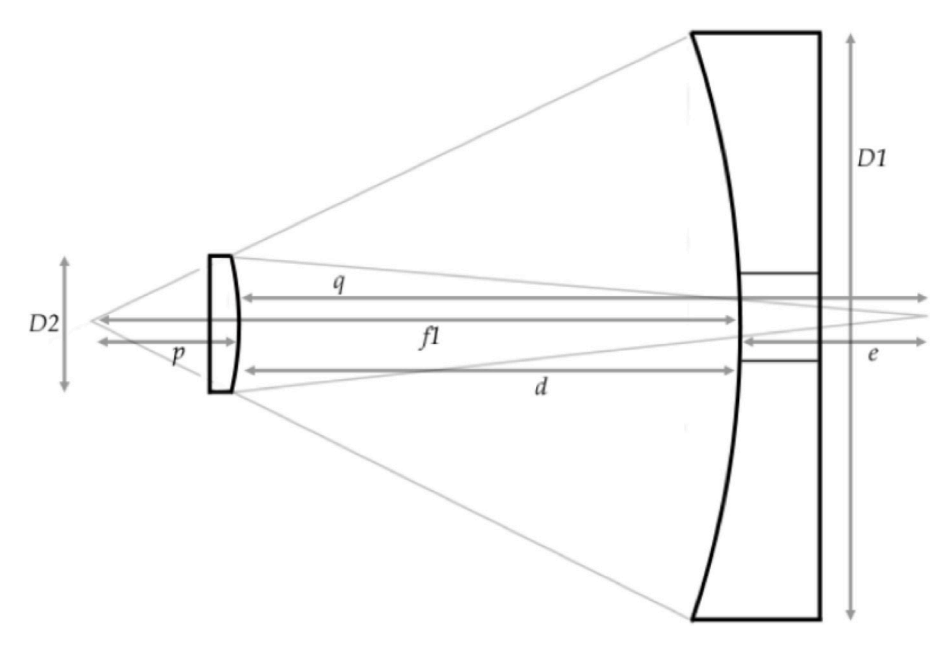


Fig. 2. R-C telescope schematic [22].

effective) focal length for a GEO space telescope with 1 m spatial resolution. Thus, of the two broad categories of reflecting telescopes, a Cassegrain is considered most feasible. The R-C telescope design uses hyperbolic mirrors for both primary and secondary mirrors whereas the classical Cassegrain uses a parabolic PM. This design is free of coma and spherical aberration, making it well suited for wide field and photographic observations. It is commonly used in large professional research telescopes, including the HST. The catadioptric variant is also compelling as its spherical mirrors are cheaper and easier to manufacture. However, its corrector lens is of nearly the same size as the PM, which drives up costs and also requires robotic OOA. Simiarly, alignment challenges in three-mirror option telesocpes increases control complexity and is thus also considered inappropriate for the end-game telescope. Thus, the R-C design is chosen for this telescope. Next, we derive the specifications of the telescope that will inform the mission and robotic OOA architectures.

Fig. 2 [22] is a schematic of a typical R-C telescope, where:

- D1 and D2 are PM and SM diameters, respectively;
- f1 is focal length of PM;
- *d* is the separation between the PM and SM;
- \boldsymbol{q} is the separation between the SM and focal plane;
- e is the separation between the PM surface and focal plane; and
- p is the distance from SM to focal point of PM.

Additionally, the magnification of an R-C telescope is defined as $M \triangleq q/p$; it is a dimensionless parameter. M also encodes information regarding how much the effective focal length can be folded relative to that of the PM; it ranges between 3 to 15 for Cassegrain configurations.

Given D1, D2, M, and the system's effective focal length, f, the goal is to determine p, q, e, d, and f1. Note that D1 and f were determined earlier to be 25 m and 50.4 m from the user requirements, respectively. We make an assumption regarding a reasonable size for the secondary (D2) to be 2.4 m; the rationale here is that it is feasible to manufacture a space-grade monolithic mirror of this size (evidenced with HST). Lastly, M=10 is assumed in the calculations and the central opening in the PM is assumed to be \sim 5.5 m in the case of the proposed large aperture telescope on account of its assembly around a central hub spacecraft. Thus, regardless of the separation between the two mirrors, the 2.4 m SM does not block the PM.

For this telescope, the PM's focal length is

$$f1 = \frac{f}{M} = 5.04 \text{ m} \tag{4}$$

and distance separating this focal point from the SM is

$$p = \frac{D2}{D1} f 1 = 0.48 \text{ m}. \tag{5}$$

To determine d (the separation between the primary and secondary mirrors), we first find q,

$$q = \frac{M}{p} = 4.84 \text{ m}$$
 (6)

and ϵ

$$e = p(M+1) - f1 = 0.28 \text{ m}$$
 (7)

and then, d=q-e=4.56 m. This separation distance of the two-mirror telescope is lower than the focal length of the Newtonian design, underscoring the former's desirability from an engineering feasibility standpoint. For this telescope, a deployable mast shall permit accurate positioning of the SM relative to the PM. In the next section, the full OTA is studied from a systems perspective and an initial technology assessment is performed for its various subsystems.

2.2. Optical telescope assembly: Technology considerations

A R-C OTA comprises four main structural elements, as shown in the exploded view of the system in Fig. 3. They are:

- segmented PMA, which is discussed in Section 2.2.1;
- modular backplane structure (supports the PMA), which is discussed in Section 2.2.2;
- deployable SM with baffles, which is discussed in Section 2.2.3;
- FPA with baffles, which is discussed in Section 2.2.4.

Each aspect is discussed in further detail below and the sizing of this OTA is summarized in Table 5 to conclude this section on space telescope design.

2.2.1. Segmented PMA

Building telescopes using monolithic mirrors present many challenges, which typically grow rapidly as their size increases eventually making their use impossible. Some key issues are [23]:

- 1. reduced availability of mirror blank material;
- 2. passive support of mirror results in large optical deflections;

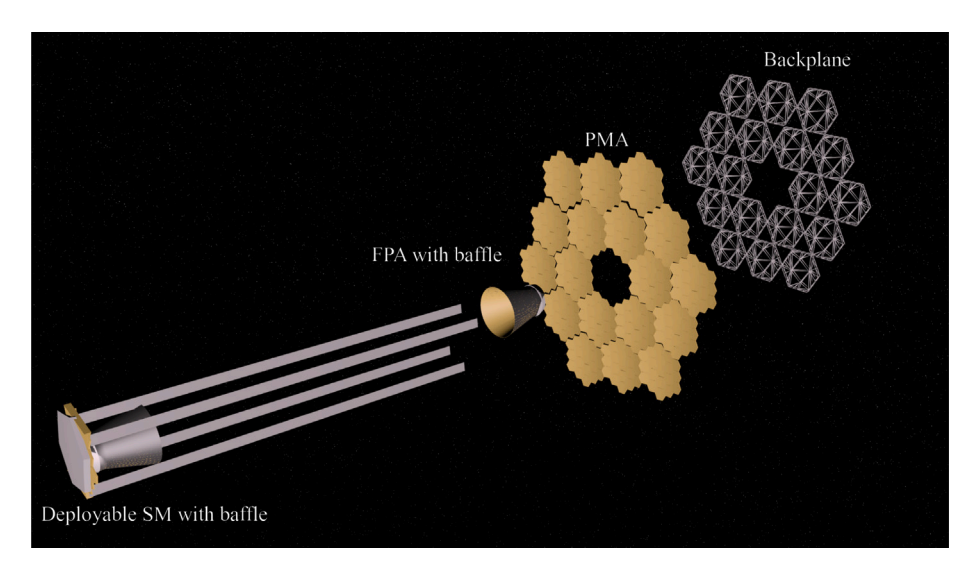


Fig. 3. Exploded view of 25 m end-game telescope.

- 3. higher risk of breakage from mishandling of larger mirrors;
- larger mirrors are subject to larger deformations from thermal changes;
- vacuum chamber for mirror coatings becomes very large and expensive;
- 6. tool costs at all stages (fabrication and handling) are high;
- 7. shipping is difficult; and
- 8. large space-based telescopes are crippled by limitations imposed by launch vehicles' fairing size.

Thus, smaller segmented mirrors are often utilized to create a larger PM for earth- and space-based observatories. Their advantage is in their ease of fabrication, transportation, installation, and maintenance when compared to a monolithic mirror (equivalent in size when the smaller mirrors are assembled). However, using segmented mirrors present their own unique challenges in manufacturing, performance, and their sizing/packing for robotic OOA. These are discussed below.

Mirror manufacturing technologies. In telescopes, a mirror substrate serves two purposes: support the thin reflective coating (approximately a few hundred atoms thick) and provide structural support. When observing in the visible and infrared (IR) wavelengths from geostationary orbit, the Sun-facing side of telescope is exposed to high temperatures and the other side to the intense cold of space; silver and aluminium are options for mirror coatings that can operate across steep temperature gradients. Aluminium is considered the better candidate to sliver as it does not tarnish as easily on the ground [24], explaining its use in the HET.

Space telescopes mirrors must have a low coefficient of thermal expansion (CTE) and be lightweight; silicon carbide (SiC), Ultra-Low Expansionx glass (ULE), beryllium (Be), carbon fibre reinforced plastic (CFRP), and ZERODUR are common substrate choices here. Based on discussions first presented in [21,25], the consequence of using these materials is summarized below and a suitable mirror material for proposed GEO telescope is identified.

- CFRP has the lowest contraction ratio at the anticipated operational temperatures (-100 °C to 125 °C for exposed mirrors [26]) in space. Though segments up to 1.5 m have been manufactured, it is difficult to meet the tight surface requirements for space observatories (a key reason for choosing beryllium mirrors in the JWST [27]). Thus, it is not considered as a candidate for the telescope in this study.
- SiC is a potential mirror substrate candidate for the end-game telescope as it is inexpensive to produce, and can be easily

formed into unconventional shapes. SiC's biggest advantage is its very high specific stiffness. Specific stiffness is defined as E/ρ , where E is Young's modulus and ρ is the mass density. Ideally, lightweight mirrors should be constructed from something that has a large E (takes lots of stress with little strain) and a low density (lightweight for its size).

SiC presents several challenges, as well. First, the material is very hard, and this makes the polishing effort difficult and time-consuming. Also, no SiC parts have been fabricated at scales larger than 0.5 m presenting a significant hurdle to overcome for their use on larger aperture telescopes [25]. SiC may also face adoption challenges from the space mirror community as it lacks the proven legacy of ULE and Be. There are currently few funded projects that use a SiC mirror [28–30]. Lastly, because so few mirrors have been created, their long-term suitability is as yet unknown but they remain a material of interest [31].

- ZERODUR is a glass/ceramic mirror substrate material, manufactured by Schott, that has a very low CTE. They were thus considered as an option for space telescopes and have been tested for a deep space mission (Deep Impact) [32]. They remained at or below 0.035 of the root mean square (RMS) figure over the 170 K cool-down from room to operational temperatures in deep space for the mission, indicating its suitability for the GEO telescope. The US Air Force Large Active Mirror Project has demonstrated a 4 m actively controlled segmented PM operating in a vacuum environment (although at 300 K); this mirror has an areal density of 140 kg/m². This makes ZERODUR® a good candidate for the GEO end-game large aperture telescope at this time but it is not a lightweight option.
- ULE has been used for the mirrors on the HST and Kepler telescope. The HST mirrors have an areal density of 180 kg/m² making it approximately ten times heavier than the beryllium mirrors on the JWST. However, a new generation of ULE was recently studied at the University of Arizona [25]; the resulting substrate material prototype had an areal density of 21 kg/m². Glass has generally been the legacy material for mirror substrates as it is thermally stable; it can be engineered into a stiff structure with minimal residual stress; and the face sheet can be polished to a high-quality optical surface.

This makes ULE a highly attractive choice as the mirror substrate material for the end-game telescope. The sizes of substrates manufactured for University of Arizona, by Composite Optics in San Diego, range in size from 0.5 m to 2 m. Interestingly, the areal density of the 2 m mirror is 13 kg/m²; it was manufactured as

part of mirror technology studies for the JWST. This makes it a more viable option than Be which is difficult to mine (and thus more expensive) and toxic. The costs for these mirrors were not published but it is important to note that areal densities may further be reduced for glass as the related manufacturing technologies mature.

• Be is a particularly desirable material for mirrors as it has a low areal density of 20 kg/m². In comparison to the low areal density ULE studied in [25], fewer actuators are necessary because Be is much stiffer than glass; it is five times stiffer than ULE and six times greater than aluminium. Be's biggest advantage as a mirror substrate is its high specific stiffness. Verbatim from [25]: "Beryllium is one of the stiffest, lightest materials that mirror-making money can buy". It has a near-zero CTE when used below 100 K which makes it an ideal material for cryogenic mirrors. This combination of properties makes Be a suitable candidate for the end-game telescope's mirrors.

However, it also has some important disadvantages. Firstly, its stiffness makes it very time-consuming to polish. Be also has a very low yield stress and cannot be stressed much before it does not spring back to its initial shape. Also, the particulate form of Be is toxic, so it must be polished and tested in special, controlled environments; this drives up manufacturing costs. Finally, there is not the established legacy for Be as there is for ULE (which will change once the JWST launches). As such, few manufacturers have the tooling and experience needed to successfully polish Be. All of these factors mean that Be is several times more expensive to work with than ULE.

• Ideal GEO telescope mirrors were also briefly discussed in [25], which states that the Earth-imaging community has determined that a successful mirror for persistent imaging from GEO must have an areal density of 5 kg/m². However, more recent discussions indicate that while areal density is a critical criterion for mirror material selection, it is not the sole criteria as there are threshold values for it at which mirrors do not survive launch loads; in other words, reducing the areal density reduces mirror stiffness that leads to its failure at launch. For this reason, JWST mirrors had their areal densities increased from 18 kg/m² to 28 kg/m² [21].

So, from this discussion it is apparent that there are two key characteristics that are taken into consideration when selecting mirror materials for space telescopes: their stiffness and areal density. Low areal density result in low mass, offering two options from the above list of choices: the new generation of ULE and Be, both of which have an estimated areal density of 20 kg/m², which can be sufficiently increased for the mirrors to survive launch loads.

However, as discussed above, these materials do not have comparable stiffness; Be is five times stiffer and has a low CTE. Also, Be requires fewer actuators than ULE. This increase in actuation also provides more control authority for maintaining a mirror's surface figure (which is why glass mirrors are sometimes referred to as high-authority mirrors [25]), which is important for EO systems. [21] speculates that, in contrast to astronomical observatories, an EO system may require a mirror with high authority control due to the mechanical and thermal dynamics of the chosen orbit. As telescopes operating in LEO are prone to more thermal cycling than a telescope at GEO, ULE might be more appropriate for the former class of EO systems whereas Be is likely be better suited in the latter case. However, a conclusive statement on the level of authority required at LEO and GEO can only be determined via practical testing on the ground in thermal vacuum chambers. For the mission analyses in this study, the state-of-the-art indicates that areal densities of 20 kg/m² are achievable with either Be or ULE, which is what is assumed for all the missions defined herein unless otherwise stated. As the Be substrate possesses superior areal density leading to lightweight mirrors without compromising stiffness, its use is assumed in all of the telescope missions analysed here; Be is now space-qualified on the JWST whereas the lightweight ULE is yet to be qualified.

Wavefront sensing and control. For a segmented PMA in a telescope to deliver an image quality comparable to a monolithic imager, the segments need to be [33]: co-aligned (stack the images produced by each segment), co-focused (ensure that focal length of each segment is the same), and co-phased (no 'piston' discontinuity between the edges of neighbouring segments). The image quality of a segmented telescope is affected by segment misalignment errors in the PM; achieving optical performance comparable to a monolithic PM requires phasing of segments to an accuracy that is a fraction of the observed wavelength. In the case of segmented optical telescopes, precision in error sensing is of the order of tens of nanometres ($\lambda/14$) and nanometre-level motion control is needed for the alignment of each mirror segment [25]. The subsystem responsible for achieving this perfect mirror alignment is known as the wavefront sensing and control (WFSC) subsystem; its objective is to reduce the wavefront error and is thus one of the most crucial subsystems of an operational telescope. Wavefront and phasing sensors are used to detect wavefront error (a measure of position error of the mirror) which is fed into the control system that computes appropriate actuation commands to reduce piston errors.

Wavefront and edge sensors: Diffraction limited imaging is achieved at wavefront RMS errors that are less than $\lambda/14$, which gives a Strehl ratio of 0.8 [34]. Wavefront sensors detect the errors with enough sensitivity and the Shack-Hartmann sensor is one such wavefront sensor that reaches an accuracy of about $\lambda/40$; a reference light source within the Shack-Hartmann sensor generates a reference wavefront which is used to provide an error measurement to the control system. These sensors have been successfully used for the phasing of the Keck telescopes and were also to be used in the Autonomous Assembly of a Reconfigurable Space Telescope (AAReST) [19] but only for focusing. The Zernike Phase Contrast Sensor is an alternative phasing sensor [34], which is more precise than the Shack-Hartmann sensor. Both sensors will be located on the FPA, along with the detectors; while a detailed design of the FPA is out of the scope of this work, the authors assume that the wavefront sensors could be placed within the imaging array.

In addition to phasing sensors, the WFSC subsystem will also utilize edge sensors (attached to every mirror) to measure relative displacements between segments. A control loop between these edge sensors and position actuators allows accurate positioning of mirrors; the edge sensors may drift and might themselves need periodic calibration, which is where the use of the aforementioned phasing sensors is needed in segmented telescopes. The edge sensors on the Keck telescopes are made of low-expansion ceramic glass and have an operating range of $+/-20~\mu m$ [34]. Apart from periodically re-calibrating edge sensors, these phasing sensors will also aid servicing aspects of segmented space telescopes as they provide the zero reference for edge sensors on newly integrated segments that might be part of a future servicing mission.

Position and curvature control: There are two aspects for position control of mirror segments for appropriate optical performance: position control of the segment's rigid body degrees-of-freedom (DoF) and its curvature control. Of the six rigid body DoF per segment, the two lateral translations and the in-plane rotation have much smaller impact on wavefront error and thus, position control typically addresses the three out-of-plane DoF:

- 'piston' degree-of-freedom, which is the translation along the axis perpendicular to the segment,
- 'tip', and 'tilt' degrees-of-freedom, which are rotational degree-of-freedom about two axes in the plane of the segment.

Mechanical actuators move each segment in these three rigid body DoF to appropriately align the PM surface-this is commonly referred to as 'active optics'. In the JWST, six actuators are used to provide redundancies in the event of a failure of one of the actuators [35]; the design of the actuators is based on a Stewart platform (also referred to as a 3–6 hexapod), where each actuator has a minimum step size <10 nm

Table 1
25 m PMA comparison: segment sizes, mass, and costs.

Segment size (m)	Number of segments	Mass (kg)	PMA cost (\$×109)
1	342	5923	1.77
0.5	1368	5923	1.77
0.3	4104	6402	1.92
0.2	8892	6224	1.86
0.1	34 200	5814	1.78

and a range >17.5 mm [36]. Thus, it is apparent that candidate space-qualified actuators already exist for this precision motion technology; the European-Extremely Large Telescope, which has 798 hexagonal segments in its 39 m PM, will make use of piezo and voice-coil-based actuators manufactured by PI-USA which provides the required step size (~1.7 nm) for imaging in the optical wavelength [37].

To further ensure optical stability, mirror surfaces should accurately align to the prescribed curvature of the parent mirror. One approach that is currently being proposed to facilitate this is by using deformable mirrors, which carry piezoelectric actuators on their surface; this approach, also referred to as 'adaptive optics', will soon be demonstrated in the AAReST mission. In contrast, the JWST uses an actuator subsystem for the tip/tilt/piston motion control for co-phasing and a radius of curvature actuator for shape control of each mirror segment; the latter is a strut-based flexure system that self-balances to assure the uniform loads are applied at six outer points of the mirror. The actuator is attached between the confluence of the rods and the segment centre such that the centre of the mirror may be pushed or pulled in reaction to the vertices to make small changes in the mirror radius of curvature. This allows the curvature of all eighteen mirrors to be matched to achieve the necessary optical performance. For the end-game telescope, these flexures might need in-house development or, if the deformable mirrors approach is desired, collaborations with the AAReST team (Surrey Space Centre (SSC) and California Institute of Technology (CalTech)) could be sought. The choice of technology will ultimately depend more on the optical performance in the visible spectrum (i.e. wavefront RMS errors less than $\lambda/14$) and on space heritage.

In summary, the challenges of the WFSC are both in precise measurements and actuation; given recent achievements with JWST, the precision required in regards to this aspect of space-based optical imaging is not insurmountable but still significant due to the lack of market access to these developments [21].

PMA sizing and costing. The PMA is the main driver for the mission mass given the larger PM aperture dictates the need for segmentation of the PM (which then also leads to multiple launches a major driver of overall mission costs). Be is the chosen mirror substrate material for the end-game telescope, which has an assumed areal density of 20 kg/m². From this, an optimal mirror size can be identified for the telescope from the data presented in Table 1. The areal cost for each mirror is assumed to be \$6 million/m² based on extant work on JWST [21]; it is interesting to note that the areal cost for Be mirrors used in JWST is half that for HST's ULE mirrors. It should also be noted that, for the JWST these numbers may have increased by an order of magnitude on account of the delays but, as yet, no reference can be found to ascertain this. However, these numbers are sufficient to make a decision for mirror segment size across a single substrate material.

Though a PMA made from 0.1 m mirrors is lighter than one made from larger segments of 0.5 m and 1 m segments, it is more expensive; thus, the 0.1 m segment is considered to be unsuitable for the 25 m end-game telescope. From our estimates, there are no apparent tradeoffs with respect to cost and mass between 0.5 m and 1 m segments; so our decision to choose the 1 m segment is driven by it needing significantly fewer actuators for WFSC and, in addition, the likelihood of manufacturing lighter mirrors at larger sizes [25]. Thus, the 25 m aperture PMA is made up of 342 segments of 1 m hexagonal segments.

Note that the effect of the reduced fill-factor is a reduction in the image brightness, which is captured by a parameter called 'f-number' or 'focal ratio'; f-number is the ratio of focal length to diameter and a value under 11 is believed to be acceptable for a bright image. For the various segmented designs proposed here, the f-number ranges between 5 and 5.2; for a filled aperture system, the f-number is \sim 4.

Estimating costs for large space telescopes is especially difficult given the limited real-world exemplars. Studies on segmented telescopes can however call on the recent pioneering work of the JWST team who have developed a variety of parametric cost estimation models [21,38–40]; the areal cost assumed in this paper thus derives from their work [21]. A notable research finding here is that duplication of segments reduces the mirrors manufacturing costs for the segmented PM compared to a monolithic mirror but there are no apparent savings in the PMA after it is fully assembled. They speculate that the increased complexity of the support structure of the segmented PM negates the initial savings.

To minimize the overall number of pick-and-place operations performed by the robot, the PM is divided into 18 mirror modules and each module further comprises 19 hexagonal mirror segments (1 m flat-to-flat). The full PMA is shown and the dimensions of an individual module is indicated in Fig. 4.

In addition to robotic assembly complexity, the launch vehicle fairing size also drives the design of the mirror module. Of particular importance is the internal diameter of the fairing. Most extant launchers can accommodate monolithic non-deployable spacecraft in excess of $\sim\!4.5$ m. Thus, several upcoming launch vehicles were surveyed of which two were considered for trade-off evaluation: the Ariane 64 and the New Glenn. We aim to revisit the feasibility of Starship in a future study.

In the selection of the appropriate mirror module design and launch vehicle, the following requirements were identified:

- 1. The combination of module design and launch vehicle must minimize the number of robotic pick-and-place operations.
- 2. The launch vehicle fairing must be wide enough to ensure that the mirror module shall not require a deployable systems philosophy (such as winged deployables used on the JWST).
- The fairing should provide the volume to accommodate a spacecraft bus within which the mirror modules are stowed.

Two design for a mirror module were considered: the first is shown in Fig. 4 where each module comprises 19 hexagonal segments. Here, the segments with the precision actuators are mounted on a lightweight rigid backplate that will itself interface with the backplane deployable perimeter truss modules (DPTM) (discussed in the next section). This design slightly exceeds the internal diameter of the Ariane 64, which is 4.57 m. An alternative is the second option that fits within the Ariane 64 and is shown in Fig. 5; here, each coloured set represents a submodule that, when assembled, would give the overall configuration of the 19 mirror module. Here, the central module (yellow) is the largest with flat-to-flat length of 3 m.

Though design option 2 satisfies requirements 2 and 3 stated above, it violates requirement 1; the full assembly of the 25 m telescope's PM portion (without backplane) would require an estimated nintey pick-and-place operations with this option, whereas only eighteen are required with option 1. Innovative designs for each mirror module can also be explored, such as those discussed by Feinberg et al. [41], but unless each module can accommodate more mirror segments, the requirements identified above would not be fully met.

The New Glenn, with a 6.2 m fairing and a payload-to-GTO capacity of the New Glenn is 13 metric tons, is thus the chosen launch vehicle. National Aeronautics and Space Administration (NASA)'s Space Launch System (SLS), with an internal fairing diameter of $\sim\!8$ m, would be a good candidate but will certainly be significantly costlier (likely to be an order of magnitude higher). It also is not likely to have the same

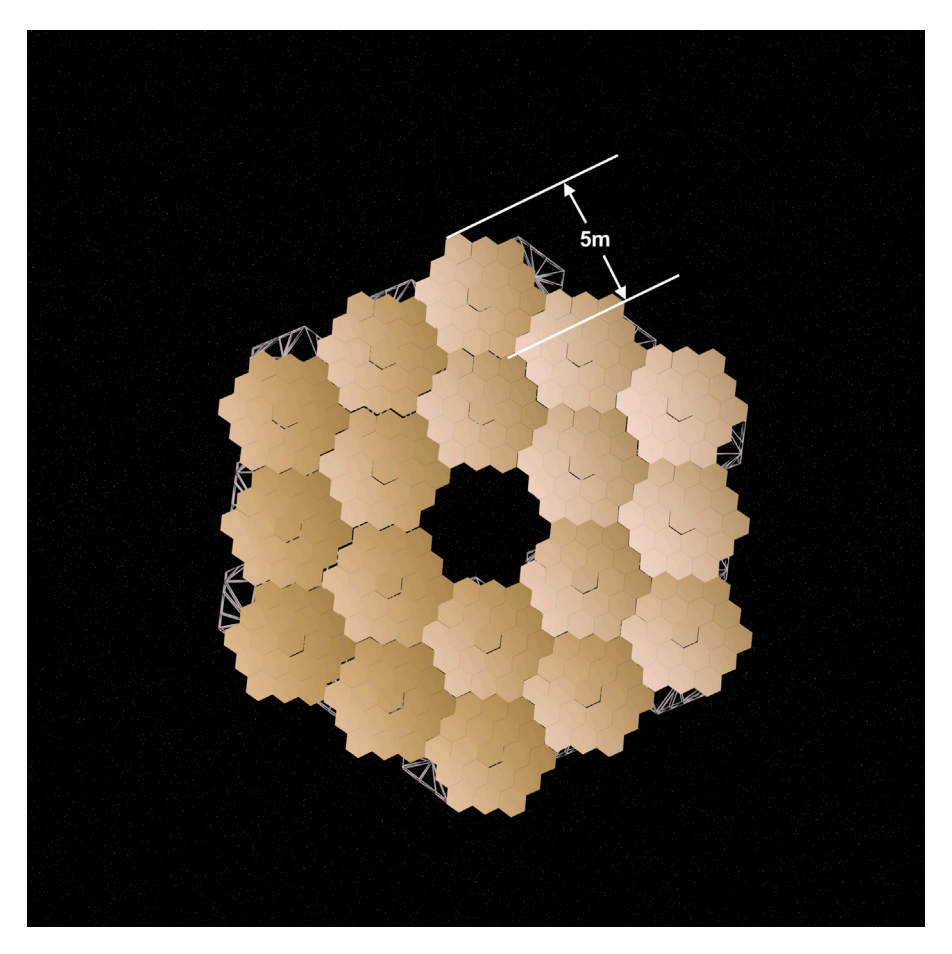


Fig. 4. Final arrangement of 18 mirror modules that make up the PMA.

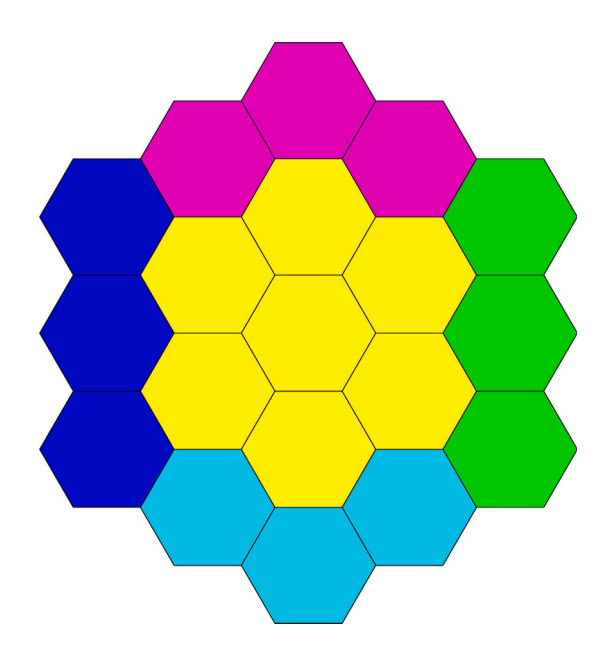


Fig. 5. Design option 2 for mirror module. (For interpretation of the references to colour in this figure legend, the reader is referred to the web version of this article.)

launch frequency, which could severely constrain the mission planning flexibility.

Table 2
Mirror module sizing summary.

Parameter	Quantifier
Number of 1 m segments per module	19
Module mass	592 kg

Table 2 summarizes the properties of the mirror module; in addition to the mass of 19 mirrors, each module mass also includes actuators and lightweight rigid backplane; their contribution is factored in for each segment as an additional 80% of segment mass.

2.2.2. Modular backplane

Assembling the backplane to accommodate the geometry of the PM surface presents the next structural challenge for the 25~m end-game telescope. Its requirements are that:

- the structural elements must stow compactly in the launch vehicle:
- 2. the full backplane must be assembled using a single manipulator; and $% \left(\frac{1}{2}\right) =\frac{1}{2}\left(\frac{1}{2}\right) =\frac{1$
- the full backplane structure must remain adequately stiff and thermally stable to satisfy the precision optical imaging requirements.

To satisfy the first requirement, a modular backplane assembled from deployable perimeter trusses was chosen. Ref. [2] identifies a hexagonal PacTruss configuration [42] to be most compatible with hexagonal mirror segment geometry and thus it was the chosen DPTM design. Note that a backplane structure could also be assembled using struts and nodes, as opposed to DPTMs; for instance, robotic assembly

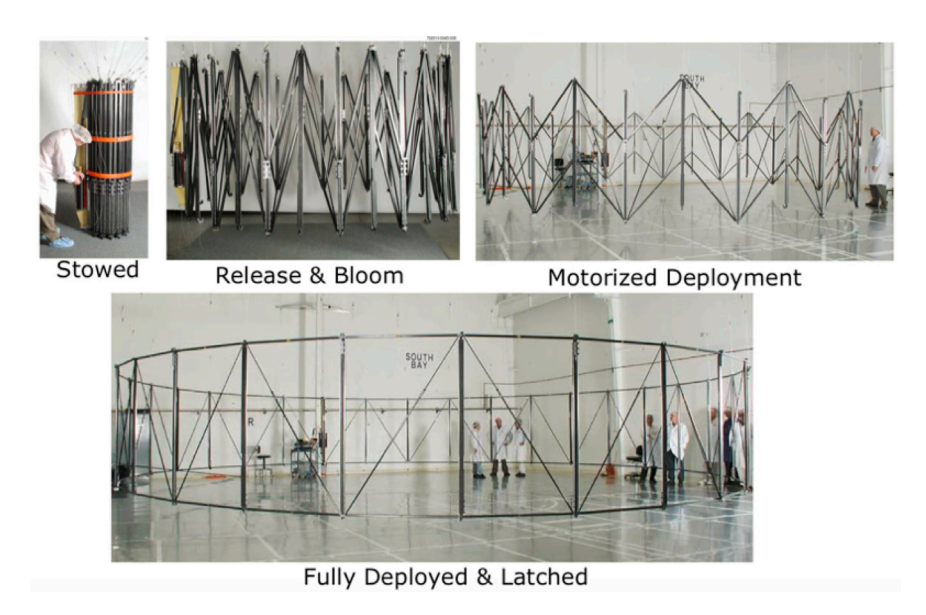


Fig. 6. Astromesh Stowed configuration (top left), Deployment phases (centre and top right), and Deployed configuration (bottom) [45].

of a truss structure, comprising 102 struts, has been demonstrated to take roughly 20 h [43]. A contrasting approach using deployable trusses would greatly reduce the number of operations in creating the backplane and are thus a more efficient approach to orbital assembly of backplanes. Constructing with struts and nodes requires more than one manipulator, violating the third requirement. It is also an antithesis to the low cost, mass, and complexity mission objectives.

The DPTM-based approach to constructing the backplane assembly relies on:

- 1. auto-deployment after attachment to the PM hub (in essence, this is the spacecraft bus) via a connector interface, or
- 2. the robot for deployment of the truss and then its attachment to the SC.

This avoids reliance on pure deployment or pure assembly of the backplane and satisfies requirement 2. Pure deployment of the supporting backplane structure requires numerous mechanisms for a large structure and present substantial mechanical challenges; e.g., mechanism actuation without jamming for large scale deployment. Ground-based testing of such large single deployable systems (i.e. one deployable backplane for the 25 m telescope) is also challenging when compared to that of smaller modules.

The DPTMs will be designed to deploy like the AstroMesh ring trusses [44] shown in Fig. 6 and demonstrated in various missions, e.g., a flexible mesh antenna was deployed, using a perimeter truss, from a stowed diameter of 0.3 m to 6 m in the Soil Moisture Active Passive (SMAP) mission. Deployed surface precision of 0.3 mm RMS error for a 9 m diameter antenna was demonstrated and is presumed to be acceptable for the modular backplane because further corrections will be provided by the WFSC system. From a materials perspective, it can be assumed that the DPTM can be constructed from either CFRP or could be 3-D printed on-orbit (when the technology is sufficiently mature). A mass of 75 kg is assumed for each DPTM [2].

Segmentation of the PM surface into identical hexagons introduces a variable gap width between segments that impacts the geometry of the backplane structure and the telescope's optical performance; thus, a key structural requirement that needs to be determined is the clearance that the truss needs so as to conform to the desired radius of curvature of the segmented PM (rule of thumb being that radius of curvature is twice the focal length). This DPTM design development is out of the scope of this study but must be pursued in a future study that builds on relevant structural requirements [46].

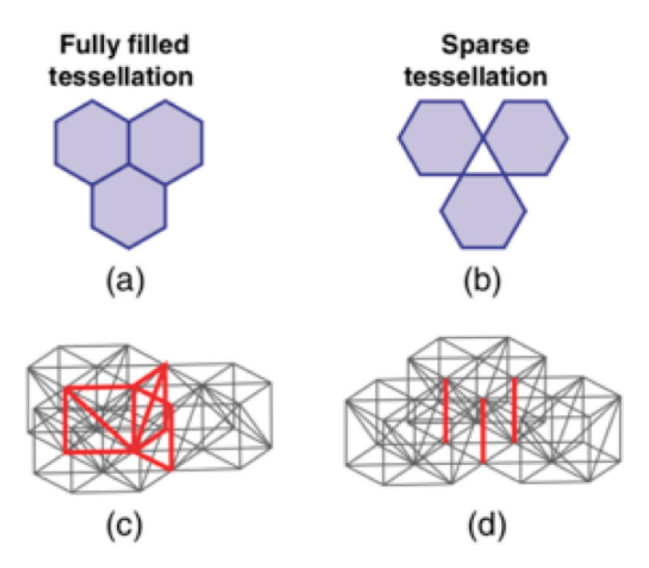


Fig. 7. Top views of (a) fully filled and (b) sparse hexagonal tessellation. Hexagonal truss modules arranged in (c) fully filled and (d) sparse tessellations; redundant members are shown in thickened red lines [2]. (For interpretation of the references to colour in this figure legend, the reader is referred to the web version of this article.)

Lee et al. [2] considered two approaches to tessellating the backplane structure assembled from DPTMs as shown in Fig. 7. A sparse tessellation for arranging the DPTMs is chosen for this GEO telescope; the justification here is that the sparse geometry includes fewer redundant truss members compared to a full tessellation [2]. Thus the orientation of each truss module remains consistent in the sparse case whereas in the fully filled case, they must alternate which side faces upward and therefore must include two different DPTM configurations for interconnects and mirror attach points. Also in a sparse tessellation of the truss backplane structure, each truss module has a hexagonal depth that is equal to the side length of the hexagon [2]; for the mirror modules, this could be ~2.5 m. Lastly, [2] tells us that the interface of such a truss with its corresponding mirror module would be at the midpoint of the outer ring of mirror segments. Note that the tessellation pattern chosen for the backplane assembly has no direct impact on the optical imaging capabilities of the system.

The complete PM backplane includes eighteen DPTMs which can be seen in Fig. 3; the trusses form two rings around a central hexagonal

hub. This hub is part of the first spacecraft launched in the assembly sequence and might include solar array attachment points that serve the PM. Of the eighteen DPTMs, the inner ring of six modules could be pre-attached permanently to the hub to aid the initial assembly process. In other words, these six DPTM would not need to be placed by the robot; they would be pre-positioned in their desired locations prior to launch and will deploy on-orbit.

2.2.3. Deployable secondary mirror

From the preceding discussion on folded telescopes, we know that the end-game telescope's SM is axially separated from the PM by 4.55 m. A resulting engineering challenge here is to actually achieve this separation in practice. One potential solution is stowed linkages in some of the DPTMs (which make up the PM backplane truss structure) to construct an appropriate support frame for the SM. Another solution based purely on deployable structures would be less risky considering its proven flight heritage when compared to assembly and meet the following requirements:

- the SM and its connecting structure should not require robotic assembly;
- 2. the overall structure should be easily stowable for launch;
- 3. the deployable structure must be rigid, thermally stable, and lightweight; and
- 4. space heritage on long-span deployable systems design must be exploited, if available.

Based on these requirements and given its demonstrated use in space at lengths exceeding the required separation distance for the endgame telescope, a deployable mast is an adequate solution. Deployable masts are a class of articulated truss that can be stowed in a small volume and expanded into long, slender, and stable booms. Their greatest benefit is their compression ratio: when packed, masts reduce to a fraction of their deployed length while being modestly wider than their deployed width. At the 4.55 m span necessary for the end-game telescope, it might be possible to achieve a precision of the order of tens of microns. Higher precision in the deployment is desirable for large focal length optical imaging systems, but it is believed that the SM will also require tens of nanometres level precision in tip/tilt/piston actuator technology to meet the optical performance requirements. The Nuclear Spectroscopic Telescope Array (NuSTAR) mission's 10 m deployable mast, used for a X-ray telescope, is the most recent example of the use of such structures in space [47]. The proposed end-game deployable mast will be based on the system used in the Shuttle Radar Topography Mission (SRTM) for radar data collection in 2000 [48], which exhibited 1 mm tip position accuracy over its 60 m span. The mast is made from CFRP, stainless steel, alpha titanium, and Invar; it consists of 87 cube-shaped sections (also called bays) with a total mass of 360 kg (the antenna systems are an additional 1340 kg). The SM is assumed to be a 2.4 m hyperbolic mirror, made of Be; based on the areal density of Be, its mass is determined to be 90.51 kg. The free-end of the truss will have the SM mounted to it, prior to launch. From an operational perspective, the truss will deploy from a canister to its full span of 4.55 m. In keeping with the 20:1 compression ratio of the SRTM mast, the canister itself will be ~0.25 m long. In SRTM, a distance measurement unit on the attitude and orbit determination avionics was used to measure the length of the mast to within three millimetres by detecting a corner-cube reflector; in the case of the endgame telescope, the WFSC subsystem could serve as this metrology instrument to monitor the mast's deployment to correct position errors via actuators.

Other options were also considered but found to not be at a sufficient level of technological maturity. For example, SM deployment could be achieved using a deployable CFRP boom with slotted hinges [49]. The current limitation of this technology is that it is yet to be demonstrated to the boom lengths desired for the 25 m end-game telescope. In the AAReST mission, the CRFP boom is 1.16 m

Table 3
Deployable mast and SM sizing.

Quantifier	Units
4.1	kg
0.7	m
7	bays
9.7	m
20:1	-
29	kg
90.5	kg
	4.1 0.7 7 9.7 20:1 29

Table 4Focal plane assembly specifications.

Parameter	Quantifier
Pixels in CMOS detector	16 megapixels
Pixel size	1.4 μm
Total number of sensors	625 sensors in 25-by-25 grid
Total sensor mass	3.8 kg
SiC backing plate mass	5 kg
FoV	100 km ²

when fully deployed [49]. Yet another approach could be formation flying the SM as proposed in Ref. [2], where Lee et al. also state that the approach is better suited for telescopes with apertures greater than 19 m as opposed to using deployables as the threshold corresponding to structural deformations exceed the limits of a typical control system. However, such an analysis is dependent on several factors such as magnification of the telescope (which drives the separation distance between mirrors). Formation flying systems also add complexity, are a potential point of failure, drive up risk/cost, and considerably increase power consumption of the mission.

Given its established flight heritage as the most rigid structure to have flown in space; its comparably higher Technology Readiness Level (TRL) to the slotted hinge mechanism and formation flying; and its not needing robotic in-orbit assembly, the mast-in-canister system is chosen to deploy the SM. The mass and length of each bay of the mast in its deployed configuration is determined from the details given for the SRTM; the resulting specifications of the mast and SM are shown in Table 3. For this study, we have assumed that another actuator technology development is not needed for positioning and shape control of the SM as actuators used for the PM segments might be sufficient.

2.2.4. FPA

The FPA is the portion of the telescope where the imaging electronics are located. Its location at the image plane also dictates where the wavefront sensors are situated to enable the wavefront sensing and control to precisely align the segmented mirrors to form a coherent surface and accurately capture images with the fully assembled telescope. In addition to the wavefront sensors, an array of CMOS detectors is also located at the focal plane. Each of these detectors has pixels of size 1.4 μ m, making them ideal for measurement of visible wavelengths. Each detector has 4096 \times 4096 pixels (16 megapixels) and there are 625 detectors arranged in a 25-by-25 array to meet the user defined field-of-view (FoV). Each detector is assumed to have a mass of 6 grams; the FPA will also include the wavefront sensors and have a total mass of 9 kg. A summary of the FPA is presented in Table 4; the assumed sensor here is the Teledyne-E2V Emerald 16M [20].

2.3. Telescope system: Block diagram and sizing summary

Fig. 8 shows the system block diagram of the space telescope. The PMA comprises eighteen DPTMs (that make up the backplane) and a corresponding number of mirror modules for the PMA; this modular and repetitive aspect of telescope components is not captured in the block diagram. The DPTMs are connected to the spacecraft structure

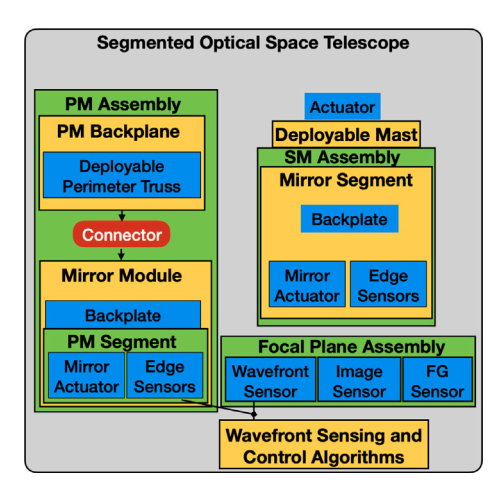


Fig. 8. System block diagram of space telescope.

Table 5
Sizing summary of 25 m telescope elements.

OTA system element	Mass (kg)	Comments
PM module	592	19 hexagonal segments with mirror actuators.
25 m PMA	10662	Made of 18 modules (342 segments).
PM backplane	1350	Comprises 18 DPTMs to support PMA.
Deployable mast	29	Supports the SM
SM	90	2.4 m monolithic hyperbolic SM.
FPA	9	Hosts the imaging and wavefront sensors

via connector interfaces; similarly, connector interfaces also enable attachment of mirror modules to DPTMs. The SM is mounted to one end of the deployable mast, which is part of the spacecraft structure. The FPA is similarly structurally attached to the spacecraft; the fine guidance sensor (FGS) also has a data link from the spacecraft's attitude determination and control system (ADCS) subsystem for precision pointing. A summary of the space telescope is provided in Table 5.

2.4. Conclusion

In this section, we determined that a 25 m space telescope would be suitable for diffraction-limited imaging from GEO to meet the baseline requirement of persistent observation with 1 m resolution. The telescope was assumed to be diffraction limited at 0.55 μm and 36,000 km was the assumed GEO altitude.

It was then seen that the fundamental driver in selecting an appropriate design for an optical space telescope is its focal length; the extremely long focal length required dictates the need to use a folded optics design. The chosen folded optics design for the space telescope is the R-C, which has four main parts:

- 1. a segmented PM,
- 2. the backplane support structure for the PMA,
- 3. a deployable SM, and
- 4. the FPA.

A comprehensive analysis on the PMA and stowing configuration for its elements was developed. The structures, such as the DPTM and mast, to which the optical components are attached are predominantly comprised of very lightweight composite material with a high stiffness-to-weight ratio and very low thermal distortion. Be was determined to be the preferred mirror material for all segments given its areal density of $20~{\rm kg/m^2}$. A cost for the entire system was developed assuming an areal cost for each mirror is assumed to be \$6 million/m². The section concluded with a block diagram of the space telescope system.

3. End-game mission analysis

In this section, a preliminary design and analysis for the endgame mission are presented. With the telescope design completed, the mission is next constrained by the following requirements:

- 1. the assembly shall be performed without generating debris;
- 2. the primary mission is to perform persistent surveillance EO from GEO with a spatial resolution of 1 m which is assumed to require a primary mirror of 25 m diameter;
- the mission shall be designed to have a nominal lifetime of ten years:
- the system shall be designed with serviceability and modularity in mind, so that it can be serviced or 'upgraded' during and/or after the nominal mission;
- the proposed mission shall comply with the UK Space Agency (UKSA) legal, licensing and regulatory framework in order to be eligible for a UK space licence (Note: This shall include UK Space debris mitigation standards); and
- 6. The estimated launch for the primary mission is 2038.

3.1. Orbit of assembly and launch vehicle

The following options were considered for assembly: GEO (the intended operational orbit) and LEO followed by a transfer to GEO. Notably, there are remarkably different thermal challenges at LEO when compared to GEO.

At GEO, while the spacecraft remains in a fixed position relative to the Earth's surface, it experiences differential heating as it presents different aspects to the Sun throughout each orbit. Further, the Earth's influence is almost negligible except for the shadowing during eclipses, which can vary in duration from zero at solstice to a maximum of 1.2 h at equinox. Long eclipses influence the design of both the spacecraft's insulation and heating systems differently. The seasonal variations in the direction and intensity of the solar input have a great impact on the design, complicating the heat transport by the need to convey most of the dissipated heat to the radiator in shadow, and the heat-rejection systems via the increased radiator area needed. Protection of optics and instruments is a key issue in the design of space telescopes and the classic approach of having highly absorbing baffles, such as those on the HST or the High Resolution Imaging Science Experiment (HiRISE) on NASA's Mars Reconnaissance Orbiter (MRO) [50], is assumed in this study for the SM and the FPA. However, a new category of reflective baffles developed for Bepi-Colombo, which tries to reject as much solar power as possible and absorb as little as possible, could be another viable alternative [51]. The protection of the primary mirror segments is considerably more challenging and an open problem: one approach could be to use a formation flying sunshield which should be designed to protect the PM segments but not obstruct the solar panels.

In summary, the thermal environment in GEO involves both seasonal variations and differential heating due to the spacecraft's orientation to the Sun. These factors must be carefully considered to ensure the thermal stability of the spacecraft during both assembly and long-term operations. In contrast, LEO experiences multiple daily occlusions, posing distinct thermal challenges that could impact mission requirements as they become more refined. This is a strong driver for performing assembly at the operational orbit. Further, the necessary ΔV to get from LEO to GEO would make this mission significantly more cost-prohibitive. Additionally, though the entire telescope could hypothetically fit in a single launch vehicle to LEO when considering mass, launches to LEO are primarily volume constrained. Thus, the sequence of assembly operations would likely necessitate more than one launch to LEO. Any rendezvous and docking (Rv&D) manoeuvre necessary between a space tug and assembled telescope for the LEO to GEO transfer would further expose the assembled PMA to undesirable damage risks that would need mitigation steps. Assembly at GEO

offers at least two important advantages: assembling the persistent EO telescope in its final operational orbit is the first of these, which eliminates the use of the tug for orbital transfer. The second is that robotic assembly process can itself be persistently observed/monitored thus increasing mission safety. On account of these reasons, assembling the telescope at GEO is the preferred option.

When accounting purely for mass delivered to GEO, either a New Glenn or Ariane 64 launch vehicle could be used for the mission. In Section 2, the New Glenn was identified as the appropriate launcher. The New Glenn's fairing capacity is better suited for a cost-effective mission to GEO and is thus the chosen launch vehicle. From a payload-to-orbit perspective, the New Glenn could achieve the assembly in four launches to Geostationary Transfer Orbit (GTO) followed by a transfer to GEO; these aspects are analysed in the next subsection. By the 2035-execution date for this end-game mission, direct-to-GEO may also be an option available with New Glenn and its competitors [52]; however, this situation is not considered in this analysis.

3.2. Propellant budget to GEO

The New Glenn rocket has a payload capacity of 13 tons to GTO; perigee raising to GEO requires additional propulsive manoeuvres. Thus, a portion of the launcher's capacity is dedicated to the propellant which can be easily determined. An assumed ΔV of 2 km/s is used to determine the propellant budget required for: orbital transfer from GTO; and station-keeping at GEO. A hydrazine/NTO bi-propellant is assumed for the GEO transfer.

3.3. Mass budgets

The geometry of the spacecraft is driven by the geometry of the payload and the New Glenn's launch fairing diameter; the latter limits the maximum permissible width of the SC ~6.2 m. Of the payload elements, the PM module is the main design driver for the spacecraft's geometry; based on Fig. 4, there are two options for the SC shape: a cube or a hexagonal prism. A hexagonal cross section is preferred for the base SC as it permits a little larger volume compared to square cross section. It also offers greater flexibility for the end-over-end walking robot to manoeuvre; and lastly, the arrangement of the inner DPTMs in the backplane structure forms a hexagonal gap in the middle. This also drives the central hub SC to be hexagonal. Note that, the volume of the DPTMs and manipulator in their stowed configurations are negligible in comparison to that of the mirror modules. In other words, their stowage is believed to not impact as heavily as the mirror modules on the launch configuration and spacecraft's geometry; this is due to the fact that the robot and DPTMs can be folded into more compact configurations when not in use.

The dry mass of the spacecraft is driven by two factors: the payload-to-bus dry mass ratio for every launch; and the beginning-of-life mass at GEO. The beginning-of-life mass is already known from the propellant budget. However, the following assumption is made regarding bus dry mass and payload elements: at beginning-of-life, the SC bus mass-to-payload ratio shall not exceed unity, as per recommendations for space mission design methodologies [26,53] and consistent with what SSTL can realize given the SSTL-42 specifications [54]. This assumption and the selected launch vehicle's delivery capabilities are formalized in Eqs. (8) and (9), respectively:

$$m_{S/C} + m_{PL} = m_{b.o.l} \tag{8}$$

$$\frac{m_{S/C}}{m_{DI}} \le 1,\tag{9}$$

where $m_{S/C}$ is the dry mass of the spacecraft bus, m_{PL} is the payload mass, and $m_{b,o,l}$ is the beginning of life mass of the system at GEO. Substituting for m_{PL} from Eq. (9) into Eq. (8) to solve for $m_{S/C}$ informs us that the spacecraft must weigh at least half of $m_{b,o,l}$; Refs. [26,53]

Table 6
S/C subsystem mass budgets as % of beginning-of-life mass at GEO.
Source: Adapted from statistical mission information discussed in [26] and [53].

Mission element	$\%m_{b.o.l}$
Payload	52
S/C dry mass (subsystem dry masses below):	48
Propulsion	6
ADCS	8
Communications	4
C&DH	1
Thermal	3
EPS	11
Structural	15

Table 7
End-game mission manifest

Launch 1	
GTO to GEO propellant mass	4962 kg
Base S/C	3358 kg
Payload (18 DPTMs, Robot, SM, FPA)	2423 kg
Total	11 785 kg
Launches 2, 3, and 4	
GTO to GEO propellant mass	6004 kg
Base S/C	3358 kg
Payload (6 mirror modules per launch)	3554 kg
Total	12 916 kg

state that the payload could be as much as 55% of the beginning of life mass. The mass budget as a percentage of $m_{b.o.l}$ is shown in Table 6, which gives a SC mass of ~3960 kg. The spacecraft subsystem masses follow discussions presented in Refs. [26,53].

From this mass budget, the end-game mission manifest comprising four launches is derived (shown in Table 7). Note that the percentage of payload mass at GEO for launch 1 is 42% whereas it is 51.4% for launches 2, 3, and 4; this is in alignment with the mass budget proposed above in Table 6. Also, though launch 1 could also accommodate 2 further mirror modules, four launches will still be necessary to assemble the PM. Thus, to maintain homogeneity in the spacecraft design and mission's ConOps, six mirror modules are delivered in each of the final three launches.

3.4. Concept of operations

Based on the four-launch mission profile described above, the assembly sequence at GEO will be as follows. The first launch will bring the telescope system's main SC bus, the RASTA assembly system, the deployable SM, FPA, and all eighteen of the modular backplaneforming DPTMs to GEO. The selected robotic assembly agent is an end-over-end walking robotic arm with seven DoF; this was chosen from a trade-off analysis between other architectures [16]. The robot attaches each stowed truss, to the base SC (for the inner ring) or to other trusses (for the outer ring), by exploiting this end-over-end walking ability to relocate itself and extract the truss from the base SC. The physical connections between the trusses, robot, and base SC are facilitated via the standardized electromechanical connector interfaces. After each truss is placed in its desired location, it auto-deploys to its unstowed configuration. Alternatively, the robot can also be utilized to unfurl the truss once it is attached to the hub. The key difference between this robotic assembly approach and the one discussed in [2] is that the truss is only deployed after it is attached to the hub in the proposed end-game mission, which creates the potential of deploying without dual-manipulators. Dual-handedness drives up the mass and cost of the robotic architecture and the mission. It also introduces unnecessary control complexity that is only now being developed for space applications through the Robotic Refueling Mission (RRM) [55]. Thus, to maintain a low degree of complexity in the robot tasks and

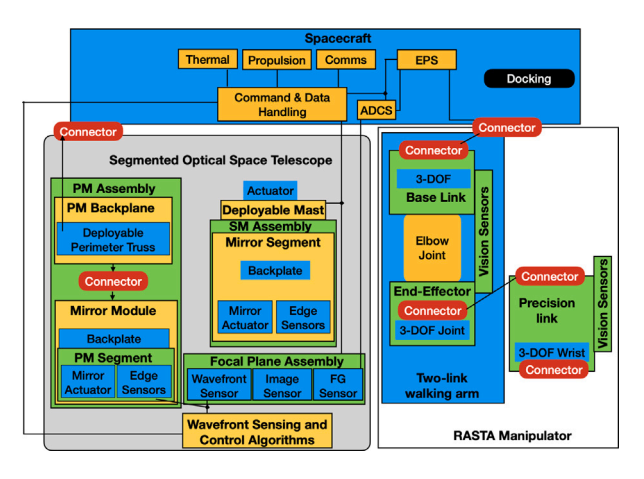


Fig. 9. End-game mission: systems block diagram.

operations, the auto-deployment approach for trusses is preferred over relying on a robotic system.

Following the assembly of the backplane, a second SC will Rv&D with the hub spacecraft to deliver six mirror modules that the robot then attaches to the deployed trusses; this corresponds to final three launches in the aforementioned mission manifest. Then the SM is deployed and the commissioning phase of the telescope will be initiated. The systems block diagram of the robotically assembled telescope is shown in Fig. 9 and full ConOps of this assembly architecture is shown in Fig. 10.

3.5. Limitations

The end-game mission architecture focusing on the OTA has been developed but there is a considerable gap in operating this telescope: the design and development of an appropriate sunshield to maintain the optical structure at a constant (or near- constant) temperature needs addressing. Deployable systems attached to the JWST sunshield were fraught with issues and might thus be unsuitable for larger telescopes [14]. The iSAT study [14] assumed modular robotic assembly of a sunshield at SEL2 but speculates it might be non-viable given that robotic manipulation of soft goods on sunshields is not well understood. Lee et al. [2] proposed the use of a formation flying deployable sunshield. This approach sounds reasonable at SEL2 as both celestial bodies are always on the same side of the spacecraft. Our speculation is that this approach might work for the GEO telescope but requires a deeper investigation on the sunshield system. Such a study would evaluate appropriate deployment approaches and mechanisms for the sunshield while also considering the development of formation flying requirements such as separation distance between the shield and telescope, which would help uncover an appropriate size of sunshade. Further, solar radiation pressure force on the shade will be countered by thrust; the resulting exhaust will impinge on the telescope so the separation distance and orbit design needs more work. These matters might also have knock-on effects on the telescope's pointing systems. Clearly sunshades are an area needing much more attention and innovative solutions as, like many other aspects of robotic OOA, the problem is an unprecedented one.

4. Roadmap of demonstration missions

A set of three missions are proposed here, which present a phased build-up of capabilities towards the end-game mission.

4.1. Mission 1: Testing of space robot in LEO

4.1.1. Mission requirements

The primary objective here is the on-orbit qualification of a robotic system and standardized grappling/connector interface; specifically, this mission will test the robot arm's ability to use its sensor systems (cameras and light detection and ranging (LiDAR)) to identify a co-operative target (i.e., the standardized connector) and then autonomously plan/execute a manoeuvre to grapple the connector. This experiment is similar to the Manipulator Flight Demonstration experiment performed by Japanese Aerospace Exploration Agency (JAXA), where an Orbital Replacement Unit (ORU) was manipulated [56]. The user requirements for the proposed mission are as follows:

- The mission shall be a robotic arm and connector demonstrator in LEO to enable a future OOA-based EO mission.
- 2. The SC shall be compatible with a low-cost launcher (as either a primary or secondary payload).
- 3. The total mass of the launched system must be under 150 kg so as to meet secondary payload requirements.
- 4. The mission shall launch by 2027.
- 5. The orbit shall be circular with an altitude lower than 400 km (i.e., lower than the altitude of the ISS).
- The proposed mission will comply with the UKSA legal, licensing, and regulatory frameworks in order to be eligible for a
 United Kingdom (UK) space licence (Note: This shall include UK
 space debris mitigation standards).

The ConOps for this mission is described in Fig. 11, which shows a set of four connectors on the base of the SC for the robot to relocate itself; however, for a simpler demonstration, it is envisioned that two connectors will be sufficient and the robot can demonstrate attaching, detaching, and re-attaching between two connectors. Demonstrating end-over-end walking with additional interfaces would be a minor-extension to the mission operations and one that would significantly advance the capabilities of the robotic system for subsequent demonstration and end-game missions.

4.1.2. Sizing

An appropriate platform for such a test would be the system designed in Ref. [57] within SSC; the system comprises a 12U SmallSat of 19.7 kg with a small robotic arm (~3.3 kg) mounted upon it; as an alternative, the fig/Demonstration of Technology-4 (DoT-4) [58] platform of 35 kg is another candidate for the SC bus. The robotic arm in Ref. [57] has a full span of 0.5 m and a mass of under 23 kg (without sensors). An external vision system mounted on the SC will enhance the situational awareness for safe manipulation by and relocation of the robot. In addition, a sensor suite will also be required on the robot end-effector for its relative navigation to the cooperative target object. A hybrid optical sensing system [59] is assumed to be appropriate for this external sensor package. Two such packages on the perimeter of the SC, each weighing 4 kg [59], and a connector are estimated to be roughly 13 kg. A potential candidate for the end-effector sensor is the Intel RealSense RGB-D sensor [60], which weighs under 10 g but is yet to be space qualified. The total payload mass (sensors, connector, and 3.3 kg robot arm) is approximately 16.4 kg. Assuming a bus mass of 19.7 kg (as per [57]) gives a mass ratio of payload to SC of 0.83 and a total mass of 36.1 kg.

There are several launch options for this mission. The envelope of the 12U satellite (0.3 m \times 0.2 m \times 0.2 m) along with the robot arm would be well within the permissible envelope of an Evolved Expendable Launch Vehicle (EELV) Secondary Payload Adapter (ESPA) system [61]. It might however be more amenable to the miniSHERPA system, which is for SC under 50 kg and a volume of 0.4 m \times 0.4 m \times 0.6 m [62]; the mini-SHERPA is a space tug with a commercial derivative of the ESPA Grande ring for deploying small payloads. A Polar Satellite Launch Vehicle (PSLV) 'piggyback' should also be

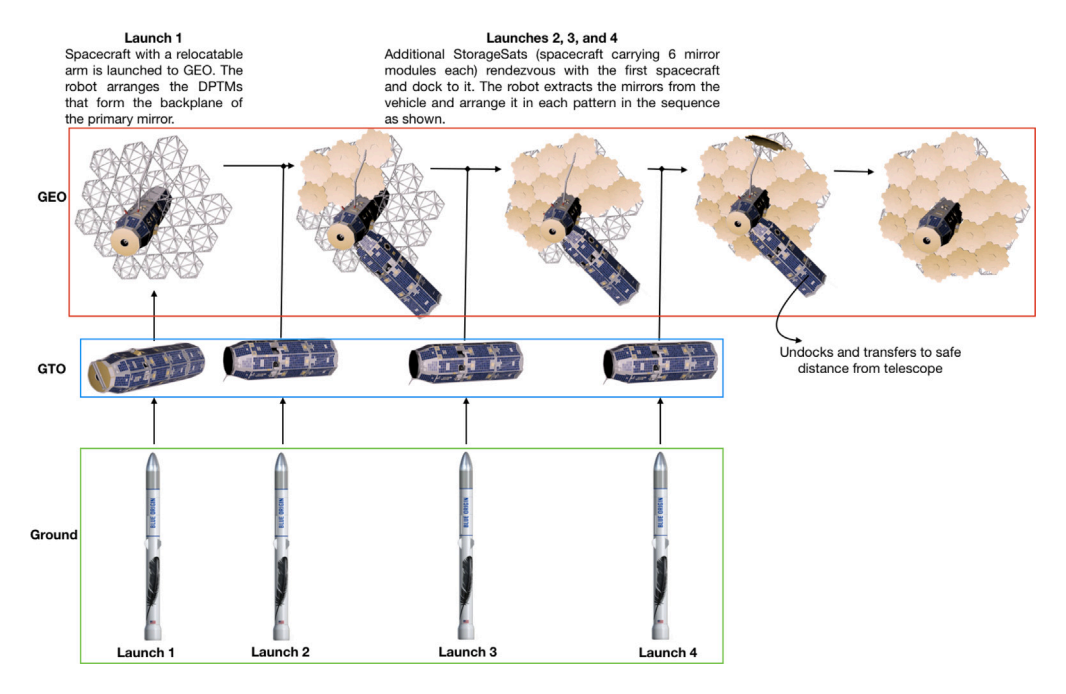


Fig. 10. ConOps of the assembly of the PM of the telescope.

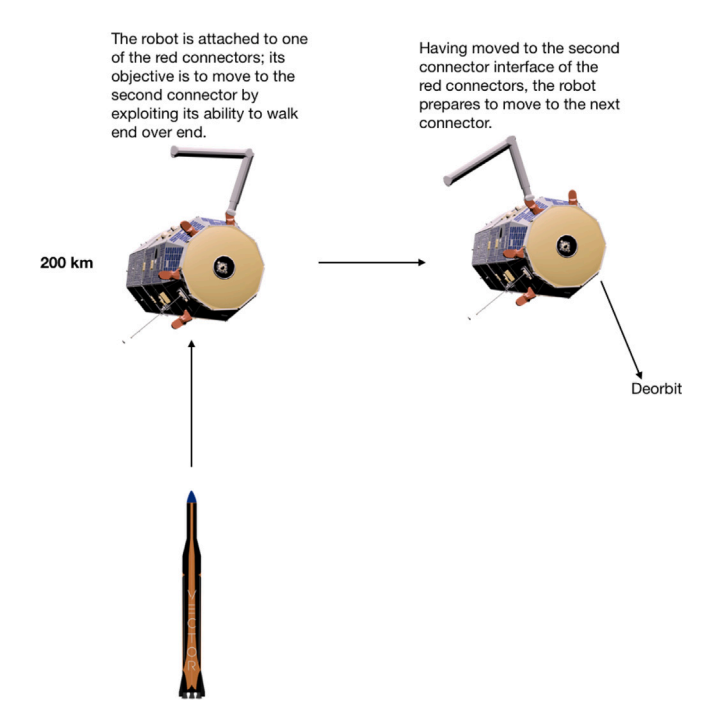


Fig. 11. ConOps of Mission 1, demonstrating the end-over-end walking robot system.

evaluated for this mission though information on its payload volumes were not available in the open literature. The Vector-R is the chosen launch vehicle (as shown in Fig. 11) as it is capable of placing up to 60 kg in LEO at an estimated launch cost of \$1.5 million which the authors consider a reasonable and competitive launch cost.

4.2. Mission 2: 2 m telescope at LEO

4.2.1. Mission requirements

The primary objective of mission 2 is to demonstrate the robotic OOA of a HST-class imager in LEO. The mission requirements are:

- Perform the assembly of a keyhole-class telescope without generating debris.
- 2. All manipulable objects are assumed to be cooperative, i.e. they communicate their pose to the robotic system so as to facilitate their manipulation.
- Develop an architecture that aligns with the architecture needed for the end-game while also building on the capabilities of the first mission demonstrating the robot and connector interface.
- 4. The mission shall be compatible with a low-cost launcher.
- 5. The proposed mission shall comply with the UKSA legal, licensing, and regulatory framework in order to be eligible for a UK space licence (Note: This shall include UK space debris mitigation standards).
- 6. The estimated launch for the primary mission is 2030.
- 7. The mission will be situated in LEO, at an altitude of 400 km.

4.2.2. Telescope design

For the purpose of this study, spatial resolutions of 0.05 m from 200 km or 0.15 m from 500 km Sun Synchronous Orbit (SSO) qualify a telescope to be of 'keyhole' class. Assuming an identical detector to that used in the end-game missions and the aforementioned resolutions, the focal length for a keyhole telescope at either altitude is ~11.2 m and 9.3 m, respectively; the corresponding aperture sizes for the primary mirror are 2.68 m and 2.24 m, respectively. To normalize the comparison between the telescopes being constructed, the mean of these apertures is chosen for the LEO telescope's PM (i.e., 2.4 m) to perform the necessary trade-off between an approach with pure pickand-place and one that involves Rv&D (i.e., an approach with at least two free-flyers to achieve telescope assembly). Given the considerably large focal lengths, once again a folded-optics R-C design is adopted for the telescope. In the subsequent design of the R-C system (based on equations presented in Section 2), a magnification factor of 10 is assumed in determining the telescope's physical attributes. Also, the SM is assumed to be hexagonal with 0.4 m flat-to-flat. The deployable mast for such a telescope will comprise two bays, with a total mass of 8.28 kg. The FPA is assumed to comprise 16 CMOS sensors arranged in a 4-by-4 grid giving a FoV of 0.28 degrees (2.45 km²) and a total mass (including SiC backing plate) of 0.23 kg.

The PMA is assumed to be made from 0.8 m segments (six in total); the assumed areal density of the mirror is 60 kg/m^2 , resulting

Table 8
2.4 m LEO telescope summary.

Parameter	Characteristics
Desired spatial resolution	0.05 m at 200 km
Focal length	10 m
PM aperture	2.4 m
SM aperture	0.4 m
Primary-secondary separation distance	1.67 m
FPA distance behind PM	0.83 m
Number of segments in primary	6
Areal density of mirror material	60 kg/m ²
Total mass of primary mirror	199.54 kg
Fill factor	0.82
Robotic agent mass	31 kg

in a 33.26 kg mirror segment. A higher areal density is used here, when compared to the end-game mission, to account for the lack of commercial access to JWST-class lightweight mirrors. The total mass of the PMA, including an allotment of 80% of the mirror mass for the actuators and backing plate per segment, is 359.19 kg. Each mirror module with actuator in the PMA is assumed to be about 0.45 m in wide and 0.8 m long. Here, the standardized connector interfaces must be integrated into the design and there shall be at least two such interfaces per module: one to facilitate manipulation by the robot arm and the other to connect the module to the DPTM. The backplane is made of 6 such DPTMs, at a total mass of 42 kg.

4.2.3. Robotic system

The robot arm in this case shall be identical in design to that proposed for the end-game mission: a two-link end-over-end walker with seven DoF and a smaller one for dexterous tasks that attaches to the larger span two-link walker. Each link on the larger robot will be 0.45 m and made of polyether ether ketone (PEEK). The link for the smaller attachable arm will be 0.2 m, giving the robotic system a full span of 1.1 m when all three links are connected. This is presumed to be sufficient to manipulate the 0.8 m segments but will need to be clarified in a future study. The mass of the robot's links and sensors is estimated to be 25.5 kg. Note that, at these smaller length scales, a two-link arm for dexterous manipulations may be sufficient. However, developing capabilities that facilitate realizing the end-game mission are prioritized and so a three-link design is retained for this demonstration mission.

4.2.4. Launch vehicle selection and mission sizing

The specifications of this LEO imager are summarized in Table 8. The total payload mass of 449 kg (including the robot), the assumed mass ratio between the payload and SC, and the desired launch vehicle determine the SC sizing/design in this case. The SC mass is derived based on the budgets presented in Table 9.

Based on a survey of launch vehicles [63], the Firefly Alpha [64] is identified as the most appropriate launcher for this SC given its ability to place systems at either 200 km or 500 km LEO. Though the PSLV was also considered, two launches of the Firefly Alpha cost less than a single PSLV launch [63]. The Firefly's fairing can fit a fully assembled telescope of under ~2 m but the 2.4 m telescope will require assembly. It was also determined that the fairing capacity will be sufficient to permit a SC that stores mirrors within it (along with the more negligible volumes of the DPTM, robot, and deployable SM). The capability to store mirrors offers protection during launch and separation, thus making it more preferable than a deployment-based approach. Note that, as the Firefly has the capacity to lift 1000 kg to 200 km or 630 kg to 500 km, two mission scenarios are possible. In the first scenario, a single launch could bring all telescope components and robot to 200 km for assembly; alternatively, a two-launch approach can be used to assemble a telescope at LEO, which would also require Rv&D of two SC.

Table 9
Assumed S/C subsystem mass budgets as % beginning-of-life mass at LEO.

Mission element	$\%m_{b.o.l}$
Payload	53
S/C dry mass (subsystem dry masses below):	47
Propulsion	1
ADCS	8
Communications	4
C&DH	1
Thermal	3
EPS	15
Structural	15

Table 10 LEO mission manifest option 1: Single launch to 200 km

and imposed mannest option 11 ombie manen to 200 mm		
LEO telescope at 200 km		
Base S/C	470 kg	
Payload (6 DPTMs, Robot, SM, FPA)	449 kg	
Total	919 kg	

Table 11
LEO mission manifest option 2: Two launches to 500 km.

Launch 1	
Base S/C	296 kg
Payload (3 DPTMs, 3 PMs, Robot, SM, FPA)	248 kg
Total	544 kg
Launch 2	
Base S/C	296 kg
Payload (3 DPTMs, 3 PMs)	201 kg
Total	497 kg

Manifests for both mission options are shown in Tables 10 and 11, respectively. In regards to choosing an appropriate architecture, the single launch approach is chosen as it is both cheaper and also enables higher resolution imaging. Further, as a first mission to demonstrate assembly, it is also comparatively simpler than one requiring Rv&D.

Note that in the LEO mission context, the mass budget inherently accounts for the propellant as it is only used for station-keeping manouevres and thus would not be a significantly high proportion of the overall mission mass. Thus, the propellant for station-keeping is assumed to be any remaining capacity of the launcher. Based on this, the propellant mass fraction for option 1 is 8.1%. Similarly for option 2, the propellant mass fraction for launches 1 and 2 are upto 13.57% and 21.16%, respectively.

4.2.5. ConOps

Fig. 12 shows the ConOps of the assembly of the PM. The assembly sequence of this single launch mission is similar to the end-game mission. The robot first assembles the six DPTMs along the base spacecraft using its ability to relocate; following truss deployment, the robot proceeds to place the mirrors in the appropriate locations. Upon completion of the assembly, the secondary mirror is deployed and the commissioning phase for telescope operations begin.

4.3. Mission 3: 5 m telescope in GEO

4.3.1. Mission requirements

The proposed GEO OOA demonstration mission has the following set of requirements:

- The primary mission objective is to demonstrate in-orbit assembly robotics technologies by constructing a 5 m Earth Observation telescope from GEO.
- 2. The assembled telescope shall be a scaled version of the end-game telescope.

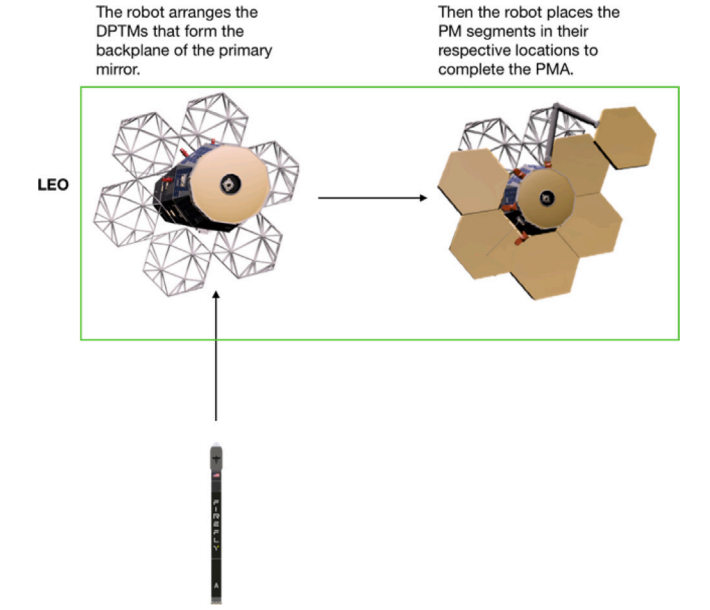


Fig. 12. ConOps LEO 2.4 m telescope assembly.

- The robotic agent used shall be a scaled version of the endgame's assembly agent.
- All manipulable objects are assumed to be co-operative, i.e. they communicate their pose to the robotic system to facilitate their manipulation.
- The proposed mission will comply with the UKSA legal, licensing, and regulatory framework in order to be eligible for a UK space licence (Note: This shall include UK Space debris mitigation standards).
- 6. The mission shall have a lifespan of ten years.
- 7. The estimated launch for this demonstration mission is 2033.

4.3.2. Telescope design

There are no specific user requirements for imaging with this mission as its primary objective is the assessment of challenges with assembling a larger telescope in the GEO environment. As this mission shall be designed to align as closely as possible to the end-game mission to identify the assembly challenges at GEO, a R-C telescope design is chosen. This 5 m optical EO telescope has a resolution of 5 m in the visible wavelength, a marked improvement to the current best GEO-based imager (Gaofen-4 has a 50 m resolution in visible wavelength [65]).

For the proposed imager, the primary-secondary separation distance is 2.01 m (this can be derived from the Cassegrain design equations in Section 2 by assuming a magnification of 10). Fig. 5, sans the centremost mirror segment, shows the schematic of the PM for this 5 m telescope, which comprises 6 mirror modules. In each module, each mirror is assumed to be of 1 m flat-to-flat length. It is evident from Fig. 5 that there are two fundamental module types (each module comprises 3 mirrors) that make up this 5 m telescope:

- Two modules, shown in blue and green in Fig. 5, represent one of the modular configurations; this is referred to as type-1 module, and
- the four sets shown in magenta and cyan make up the other type of modular arrangement and are referred to as type-2 module; the yellow module in Fig. 5 can similarly comprise two type-2 modules.

All mirror segments are assumed to be 1 m in flat-to-flat length and have a mass of 30.31 kg (assumed areal density of 35 kg/m 2). Assumed thickness of each mirror (and, therefore module) is 0.45 m.

Table 12Sizing summary of 5 m telescope elements.

OTA system element	Mass (kg)	Comments
PM module	94	3 hexagonal segments (1 m flat-to-flat) with mirror actuators.
5 m PMA	312	Made of 6 PM modules; 18 mirror segments in total.
PM backplane	270	Comprises 18 DPTMs, each of 15 kg; supports the PMA.
Deployable mast	12	Supports the secondary mirror
SM	4	0.5 m monolithic hyperbolic secondary mirror.
FPA	0.36	Hosts the imaging and wavefront error sensors

The mission is designed to replicate many aspects of the end-game assembly mission (whilst using a smaller aperture design) namely: robotically assembling groups of mirrors (as opposed to placing a single hexagonal mirror segment in every move as done in the LEO OOA demonstration mission); and constructing a telescope with more than one-level/layer of tessellation in the PMA. Just as in the end-game telescope, the mirror modules will be connected to the base-spacecraft via DPTMs that have been placed by the robot along the SC. The standardized connector interface establishes physical connections between the modules to the spacecraft and/or the arm. In total, six pick-and-place operations will be performed by the robotic arm to assemble the primary mirror (in addition to six similar motions to assemble the backplane using DPTMs). When an assembly task is out of the robot's current working volume, the robot shall relocate itself so as to resume with the assembly objective.

As with the end-game telescope design, a deployable mast system is used to deploy the SM after the PM is assembled. The FPA of this 5 m telescope is also designed to offer a FoV of $100~\rm km^2$; for this, CMOS sensors identical to those in the end-game telescope are selected and arranged in a 5-by-5 grid (i.e., 25 sensors in total). A table summarizing the sizing of the various elements of this telescope are shown below in Table 12. The mass of the DPTM here is assumed to scale linearly as a function of the deployed length of the DPTM used in the end-game telescope.

4.3.3. Robotic system

The robot shall be identical in design to that proposed for the end-game mission: a two-link end-over-end walker and an extensible smaller arm for dexterous tasks. The links on the walker will be 1 m each and made of PEEK. The link(s) for the dexterous arm will be 0.5 m. The mass of the robot arm's booms and sensors (assumed to be 20% of the total mass of the links) are found to be 53 kg.

4.3.4. Propulsion and launch vehicle selection

Three low-cost launch vehicles were considered here: Geosynchronous Satellite Launch Vehicle Mark III (GSLV-III), Ariane 62, and Falcon-9. As these vehicles only deliver to GTO, trade-offs between them was driven mainly by mass-to-GTO. As with the endgame telescope, the bipropellant hydrazine/NTO system was selected for Hohmann transfer to GEO. The sizing budget from Table 6 is assumed for these launchers with an assumed ΔV of 2 km/s; this budget accounts for the GTO-to-GEO transfer and ten-year station-keeping requirements.

It was found that the GSLV-III's beginning-of-life mass is insufficient to complete the mission in one-launch; as a multi-launch approach would drive up the cost of the mission, it is not preferred here. Though the Falcon-9 allows a generous beginning-of-life mass and a comparable fairing diameter to the Ariane 62, its fairing volume is lower. It may not be necessary to have the additional volume offered by the Ariane 62, the authors believe it provides a useful "cushion". Thus, the Ariane 62 is the chosen vehicle in developing the mission manifest shown in Table 13.

Table 13
GEO 5 m demo mission manifest.

Ariane 62 launcher	
GTO to GEO propellant mass	2309 kg
Base S/C	1291 kg
Payload (18 DPTMs and PMs, Robot, SM, FPA)	740 kg
Total	4340 kg

4.3.5. ConOps

The assembly sequence for this demonstration mission at GEO is similar to the single launch LEO OOA mission; the only difference here is that there are 12 additional DPTMs and mirrors forming the outer ring. The launch will bring the SC bus, the robotic assembly agent, and modular telescope elements to GEO. Here, the robot unpacks and assembles all the DPTMs around the base SC in a total of 18 motions. The layout of the DPTMs is identical to that of the end-game telescope, the only difference being that the demo mission DPTMs are \sim 1 m when fully deployed whereas each end-game DPTM is 5 m when deployed. After truss auto-deployment, the robot places the mirror modules, beginning from the inner segments and working its way outward.

5. Conclusions

This paper presents a first-order design of a high-resolution imaging system of 25 m aperture to meet end-user requirements. To this end, the paper began by evaluating optical telescope designs from which the Ritchey-Chretien telescope was found to be an ideal design to meet the user requirement of 1 m spatial resolution from GEO for the end-game telescope. Challenges associated with imaging in the optical wavelengths for this system were assessed, technologies needing development were identified, and a trade-offs driven mission profile for robotic on-orbit assembly were presented. Then a full mission architecture for its OOA was also presented. This paper then proposes and analyses a set of three demonstration missions, which serve to pave the way for the technology demonstrations necessary for achieving the end-game telescope assembly. One of the key limitations of the work in addressing the thermal issues at GEO of the end-game telescope. Future work will address this gap while separately analysing the mission architectures described herein by developing simulations relevant to autonomous robotic assembly. Another aspect worth exploring is the reconsidering telescope assembly at LEO as the parts could be deorbited as a means to mitigate the debris population- however, a challenge in this case would be safe deorbiting. Another option might be to increase the propellant budgets of the systems that are in GEO so as to ensure eventual deorbiting instead of relocation to a graveyard orbit.

CRediT authorship contribution statement

Angadh Nanjangud: Writing – original draft, Writing – review & editing. Craig Underwood: Supervision, Validation. Chakravarthini M. Rai: Supervision. Steve Eckersley: Project administration. Martin Sweeting: Funding acquisition. Paolo Bianco: Project manager.

Declaration of competing interest

The authors declare that they have no known competing financial interests or personal relationships that could have appeared to influence the work reported in this paper.

References

- A. Nanjangud, P.C. Blacker, S. Bandyopadhyay, Y. Gao, Robotics and AI-enabled on-orbit operations with future generation of small satellites, Proc. IEEE 106 (3) (2018) 429–439.
- [2] N.N. Lee, J.W. Burdick, P. Backes, S. Pellegrino, K. Hogstrom, C. Fuller, B. Kennedy, J. Kim, R. Mukherjee, C. Seubert, et al., Architecture for in-space robotic assembly of a modular space telescope, J. Astron. Telesc. Instrum. Syst. 2 (4) (2016) 041207.
- [3] C. Saunders, D. Lobb, M. Sweeting, Y. Gao, Building large telescopes in orbit using small satellites, Acta Astronaut. 141 (2017) 183–195.
- [4] N. Siegler, R. Mukherjee, H. Thronson, Building the future: The nasa inspace assembled telescope study, in: American Astronomical Society Meeting Abstracts# 233, Vol. 233, 2019, pp. 326–308.
- [5] R. Mukherjee, N. Siegler, H. Thronson, K. Aaron, J. Arenberg, P. Backes, A. Barto, K. Belvin, L. Bowman, D. Calero, et al., When is it worth assembling observatories in space? Bull. Am. Astron. Soc. 51 (7) (2019) 50.
- [6] M. Deremetz, G. Grunwald, F. Cavenago, M.A. Roa Garzon, M. De Stefano, H. Mishra, M. Reiner, S. Govindaraj, A. But, I. Sanz Nieto, et al., Concept of operations and preliminary design of a modular multi-arm robot using standard interconnects for on-orbit large assembly, in: Proceedings of the International Astronautical Congress, IAC, 2021.
- [7] P. Letier, X.T. Yan, M. Deremetz, A. Bianco, G. Grunwald, M. Roa, R. Krenn, M.M. Arancón, P. Dissaux, J.S.G. Casarrubios, et al., MOSAR: Modular spacecraft assembly and reconfiguration demonstrator, in: 15th Symposium on Advanced Space Technologies in Robotics and Automation, 2019.
- [8] J. Vinals, J. Gala, G. Guerra, Standard interface for robotic manipulation (sirom): Src h2020 og5 final results-future upgrades and applications, in: International Symposium on Artificial Intelligence, Robotics and Automation in Space (I-SAIRAS), 2020.
- [9] M.A. Roa Garzon, C. Koch, M. Rognant, A. Ummel, P. Letier, A. Turetta, P. Lopez, S. Trinh, I.V. Rodriguez Brena, K. Nottensteiner, et al., PULSAR: Testing the technologies for on-orbit assembly of a large telescope, in: 16th Symposium on Advanced Space Technologies in Robotics and Automation, ASTRA 2022, ESA, 2022.
- [10] M.A. Roa, K. Nottensteiner, I. Rodríguez, T. Bachmann, J.-P. Lutze, P. Letier, A. Ummel, J. Rouvinet, F. Cosandier, D. Nguyen, et al., Autonomous precise assembly of segmented mirror tiles for a space telescope, in: 2024 IEEE Aerospace Conference, IEEE, 2024, pp. 1–11.
- [11] P. Letier, T. Siedel, M. Deremetz, E. Pavlovskis, B. Lietaer, K. Nottensteiner, M.A. Roa Garzon, J. Sánchez Garcia, J.L. Corella, J. Gancet, Hotdock: Design and validation of a new generation of standard robotic interface for on-orbit servicing, in: 71st International Astronautical Congress, IAC 2020, IAF, 2020.
- [12] P. Schoonejans, R. Stott, F. Didot, A. Allegra, E. Pensavalle, C. Heemskerk, Eurobot: EVA-assistant robot for ISS, moon and mars, in: Proceedings of 8th ESA Workshop on Advanced Space Technologies for Robotics and Automation, ASTRA, Noordwijk, 2004.
- [13] A. Rusconi, P. Magnani, P. Campo, R. Chomicz, G. Magnani, C. Lambert, G. Gruener, et al., DEXARM engineering model development and testing, in: 10th ESA Workshop on Advanced Space Technologies for Robotics and Automation-ASTRA, Vol. 2008, 2008.
- [14] R. Mukherjee, N. Siegler, H. Thronson, The future of space astronomy will be built: results from the in-space astronomical telescope (iSAT) assembly design study, in: 70th International Astronautical Congress, Curran Associates, Inc Red Hook, 2019.
- [15] M.A. Roa, K. Nottensteiner, A. Wedler, G. Grunwald, Robotic technologies for inspace assembly operations, in: 14th Symposium on Advanced Space Technologies in Robotics and Automation, ASTRA, 2017.
- [16] A. Nanjangud, P.C. Blacker, A. Young, C.M. Saaj, C.I. Underwood, S. Eckersley, M. Sweeting, P. Bianco, ROBOTIC architectures FOR the ON-ORBIT ASSEMBLY OF LARGE space telescopes, in: Proceedings of the Advanced Space Technologies in Robotics and Automation (ASTRA 2019) Symposium, European Space Agency (FSA), 2019
- [17] K. McBryan, Comparison between stationary and crawling multi-arm robotics for in-space assembly, in: 2020 IEEE/RSJ International Conference on Intelligent Robots and Systems, IROS, IEEE, 2020, pp. 1849–1856.
- [18] D. Arney, J. Mulvaney, C. Williams, C. Stockdale, N. Gelin, P. le Gouellec, Inspace servicing, assembly, and manufacturing (ISAM) state of play-2023 edition, in: Consortium for Space Mobility and ISAM Capabilities (COSMIC) Kickoff, 2023.
- [19] C. Underwood, S. Pellegrino, V.J. Lappas, C.P. Bridges, J. Baker, Using CubeSat/micro-satellite technology to demonstrate the autonomous assembly of a reconfigurable space telescope (aarest), Acta Astronaut. 114 (2015) 112–122.
 [20] Teledyne-E2V emerald 16M, 2019, URL https://www.teledyne-e2v.com/
- [20] Teledyne-E2V emerald 16M, 2019, URL https://www.teledyne-e2v.com/content/uploads/2019/01/36956_Teledyne-E2V-CMOS-sensor-guide-update_Jan-19_v2_AW_SPREADS_WEB.pdf. (Accessed 28 Februarty 2019).
- [21] D. Baiocchi, H.P. Stahl, Enabling Future Space Telescopes: Mirror Technology Review and Development Roadmap, astro2010: The Astronomy and Astrophysics Decadal Survey, Technology Development Paper (23), 2009.
- [22] Lockwood optics: Ritchey-Chretien Cassegrain telescope design equations, 2019, URL http://www.loptics.com/ATM/mirror_making/cass_info/cass_info.html (Accessed 28 February 2019).

- [23] J. Nelson, Segmented mirror telescopes, in: Optics in Astrophysics, Springer, 2006, pp. 61–72.
- [24] Gemini observatory: mirror coatings, 2019, URL http://www.gemini.edu/node/ 103. (Accessed 28 February 2019).
- [25] D. Baiocchi, Design and control of lightweight, active space mirrors, 2004.
- [26] V.L. Pisacane, Fundamentals Of Space Systems, Johns Hopkins University/Appli, 2005.
- [27] L.D. Feinberg, M. Clampin, R. Keski-Kuha, C. Atkinson, S. Texter, M. Bergeland, B.B. Gallagher, James webb space telescope optical telescope element mirror development history and results, in: Space Telescopes and Instrumentation 2012: Optical, Infrared, and Millimeter Wave, Vol. 8442, International Society for Optics and Photonics, 2012, 84422B.
- [28] U. Papenburg, W. Pfrang, G. Kutter, C.E. Mueller, B.P. Kunkel, M. Deyerler, S. Bauereisen, Optical and optomechanical ultralightweight C/SiC components, in: Optical Manufacturing and Testing III, Vol. 3782, International Society for Optics and Photonics, 1999, pp. 141–157.
- [29] R. Eng, J.R. Carpenter, C.A. Foss, J.B. Hadaway, H.J. Haight, W.D. Hogue, D. Kane, J.R. Kegley, H.P. Stahl, E.R. Wright, Cryogenic performance of a lightweight silicon carbide mirror, in: Optical Materials and Structures Technologies II, Vol. 5868, International Society for Optics and Photonics, 2005, 58680Q.
- [30] H. Kaneda, T. Onaka, T. Nakagawa, K. Enya, H. Murakami, R. Yamashiro, T. Ezaki, Y. Numao, Y. Sugiyama, Cryogenic optical performance of the ASTRO-F SiC telescope, Appl. Opt. 44 (32) (2005) 6823–6832.
- [31] X. Zhang, H. Hu, X. Wang, X. Luo, G. Zhang, W. Zhao, X. Wang, Z. Liu, L. Xiong, E. Qi, et al., Challenges and strategies in high-accuracy manufacturing of the world's largest SiC aspheric mirror, Light: Sci. Appl. 11 (1) (2022) 310.
- [32] J.W. Baer, W.P. Lotz, Figure testing of 300-mm Zerodur mirrors at cryogenic temperatures, in: Cryogenic Optical Systems and Instruments IX, Vol. 4822, International Society for Optics and Photonics, 2002, pp. 35–41.
- [33] P. Bely, The Design and Construction of Large Optical Telescopes, Springer, 2003.
- [34] I. Surdej, Co-phasing Segmented Mirrors: Theory, Laboratory Experiments and Measurements on Sky (Ph.D. thesis), TU-Munich, 2011.
- [35] J.A. Gersh-Range, E.M. Elliott, M.D. Perrin, R.P. van der Marel, Minimizing the wavefront error degradation for primary mirror segments with failed hexapod actuators, Opt. Eng., Bellingham 51 (1) (2012) 011005.
- [36] P.A. Lightsey, C.B. Atkinson, M.C. Clampin, L.D. Feinberg, James webb space telescope: large deployable cryogenic telescope in space, Opt. Eng., Bellingham 51 (1) (2012) 011003.
- [37] PI-USA piezo- and voice-coil actuators, 2019, URL https://tinyurl.com/yy9bpyrb. (Accessed 28 February 2019).
- [38] H.P. Stahl, Survey of cost models for space telescopes, Opt. Eng., Bellingham 49 (5) (2010) 053005.
- [39] H.P. Stahl, T. Henrichs, A. Luedtke, M. West, Update on multivariable parametric cost models for ground and space telescopes, in: Space Telescopes and Instrumentation 2012: Optical, Infrared, and Millimeter Wave, Vol. 8442, International Society for Optics and Photonics, 2012, 844224.
- [40] H.P. Stahl, T. Henrichs, Multivariable parametric cost model for space and ground telescopes, in: Modeling, Systems Engineering, and Project Management for Astronomy VI, Vol. 9911, International Society for Optics and Photonics, 2016, 99110L.
- [41] L.D. Feinberg, J.G. Budinoff, H.A. MacEwen, G.W. Matthews, M. Postman, Modular assembled space telescope, Opt. Eng., Bellingham 52 (9) (2013) 091802.
- [42] J.M. Hedgepeth, Pactruss support structure for precision segmented reflectors, 1989.
- [43] W. Doggett, Robotic assembly of truss structures for space systems and future research plans, in: Proceedings, IEEE Aerospace Conference, Vol. 7, IEEE, 2002, p. 7.
- [44] M.W. Thomson, The astromesh deployable reflector, in: IEEE Antennas and Propagation Society International Symposium. 1999 Digest. Held in Conjunction with: USNC/URSI National Radio Science Meeting (Cat. No. 99CH37010), Vol. 3, IEEE, 1999, pp. 1516–1519.

- [45] AstroMesh deployable trusses by Northrop Grumman, 2019, URL https://tinyurl.com/astromeshDTM. (Accessed 28 February 2019).
- [46] M.S. Lake, L.D. Peterson, M.B. Levine, Rationale for defining structural requirements for large space telescopes, J. Spacecr. Rockets 39 (5) (2002) 674-681
- [47] Nustar mast, 2019, URL https://www.nustar.caltech.edu/page/paper_model. (Accessed 28 February 2019).
- [48] T.G. Farr, P.A. Rosen, E. Caro, R. Crippen, R. Duren, S. Hensley, M. Kobrick, M. Paller, E. Rodriguez, L. Roth, et al., The shuttle radar topography mission, Rev. Geophys. 45 (2) (2007).
- [49] C. Underwood, S. Pellegrino, H. Priyadarshan, H. Simha, C. Bridges, A. Goel, T. Talon, A. Pedivellano, Y. Wei, F. Royer, et al., AAReST autonomous assembly reconfigurable space telescope flight demonstrator, in: Proceedings of the 69th International Astronautical Congress, IAC, International Astronautical Federation (IAF), 2018.
- [50] D. Gallagher, J. Bergstrom, J. Day, B. Martin, T. Reed, P. Spuhler, S. Streetman, M. Tommeraasen, Overview of the optical design and performance of the high resolution science imaging experiment (HiRISE), in: Current Developments in Lens Design and Optical Engineering VI, Vol. 5874, International Society for Optics and Photonics, 2005, 58740K.
- [51] T. Beck, B. Lüthi, G. Messina, D. Piazza, K. Seiferlin, N. Thomas, Thermal analysis of a reflective baffle designed for space applications, Acta Astronaut. 69 (5–6) (2011) 323–334.
- [52] Direct insertion to GEO, 2019, URL https://tinyurl.com/yydgqm6y. (Accessed 28 February 2019).
- [53] W.J. Larson, J.R. Wertz, Space Mission Analysis and Design, Tech. Rep. Torrance, CA (United States); Microcosm, Inc., 1992.
- [54] (internally distributed), SSTL-42 spec sheet, Tech. Rep, SSTL, Guildford, UK, 1992.
- [55] RRM site, 2019, URL https://sspd.gsfc.nasa.gov/robotic_refueling_mission.html. (Accessed 28 February 2019).
- [56] Y. Ohkami, M. Oda, NASDA's Activities in Space Robotics, Vol. 440, EUROPEAN SPACE AGENCY-PUBLICATIONS-ESA SP, 1999, pp. 11–18.
- [57] L. Jackson, C.M. Saaj, A. Seddaoui, C. Whiting, S. Eckersley, The downsizing of a free-flying space robot, in: Annual Conference Towards Autonomous Robotic Systems, Springer, 2019, pp. 480–483.
- [58] SSTL media on DoT-4, 2019, URL https://www.sstl.co.uk/media-hub/latest-news/2018/sstl-announces-35kg-lunar-comms-mission-for-2021. (Accessed 28 February 2019).
- [59] S. Eckersley, C. Saunders, D. Lobb, G. Johnston, T. Baud, M. Sweeting, C. Underwood, C. Bridges, R. Chen, Future rendezvous and docking missions enabled by low-cost but safety compliant guidance navigation and control (GNC) architectures, in: Proceedings of the 15th Reinventing Space Conference, British Interplanetary Society, 2017.
- [60] Intel RealSense datasheet, 2019, URL https://www.mouser.co.uk/pdfdocs/Intel-RealSense-D400-Series-Datasheet_003.pdf. (Accessed 28 February 2019).
- [61] ESPA user's guide, 2019, URL http://www.moog.com/content/dam/moog/ literature/Space_Defense/spaceliterature/structures/Moog_ESPA_UsersGuide.pdf. (Accessed 28 February 2019).
- [62] Spaceflight Sherpa user's guide, 2019, URL http://www.spaceflight.com/wp-content/uploads/2015/05/SPUG-RevF.pdf. (Accessed 28 February 2019).
- [63] T. Wekerle, J.B. Pessoa Filho, L.E.V.L.d. Costa, L.G. Trabasso, Status and trends of smallsats and their launch vehicles—An up-to-date review, J. Aerosp. Technol. Manag. 9 (3) (2017) 269–286.
- [64] Firefly alpha user's guide, 2019, URL https://fireflyspace.com/wp-content/ themes/firefly_aerospace/files/Firefly_Aerospace_Payload_User's_Guide.pdf. (Accessed 28 February 2019).
- [65] Gaofen-4 online information, 2019, URL https://space.skyrocket.de/doc_sdat/gf-4.htm. (Accessed 28 February 2019).